Palaeontologia Electronica
palaeo-electronica.org

The first cranium of *Axestemys infernalis* (Testudines: Trionychidae) from the Lance Formation of Wyoming, USA; an updated description and phylogenetic analysis

Jasper Ponstein, Jonathan J.W. Wallaard, Maarten de Rijke, and René H.B. Fraaije

ABSTRACT

We report the first trionychid turtle skull from the Lance Formation (Maastrichtian) of Wyoming, USA, a relatively complete cranium of *Axestemys infernalis.* Included is an osteological and preliminary neuroanatomical description aided by a medical CT-scan of the specimen. Comparison with other published crania of *A. infernalis* yielded considerable intraspecific variation. Notably, our specimen does not bear an ossified premaxilla, the postorbital extends ventrally and the maxilla-jugal suture is positioned posterior to the orbit. Based on this new anatomical data, both a parsimony and a Bayesian analysis of an updated character-taxon matrix of Trionychia have been run, which found *A. infernalis* as either outside Plastomenidae+Cyclanorbinae or as an early diverging stem-cyclanorbine. Moreover, for the first time a fossil trionychid brain-case is described in detail.

Jasper Ponstein. AG Paläobiologie und Evolution, Institut für Biologie, Humboldt Universität zu Berlin, Unter den Linden 6, 10117 Berlin, Germany and Museum für Naturkunde Berlin, Leibniz-Institut für Evolutions- und Biodiversitätsforschung, Invalidenstraße 43, 10115 Berlin, Germany and Oertijdmuseum, Bosscheweg 80, 5283 WB Boxtel, Netherlands. Corresponding author. ponsteij@hu-berlin.de
Jonathan J.W. Wallaard. Oertijdmuseum, Bosscheweg 80, 5283 WB Boxtel, Netherlands. curator@oertijdmuseum.nl
Maarten de Rijke. Oertijdmuseum, Bosscheweg 80, 5283 WB Boxtel, Netherlands. maarten@oertijdmuseum.nl
René H.B. Fraaije. Oertijdmuseum, Bosscheweg 80, 5283 WB Boxtel, Netherlands. info@oertijdmuseum.nl

Keywords: *Axestemys*; Trionychidae; anatomy; cranium; phylogeny; Maastrichtian

Submission: 11 December 2023. Acceptance: 24 May 2024.

Final citation: Ponstein, Jasper, Wallaard, Jonathan J.W., de Rijke, Maarten, and Fraaije, René H.B. 2024. The first cranium of *Axestemys infernalis* (Testudines: Trionychidae) from the Lance Formation of Wyoming, USA; an updated description and phylogenetic analysis. Palaeontologia Electronica, 27(2):a31.
https://doi.org/10.26879/1361
palaeo-electronica.org/content/2024/5234-new-skull-of-axestemys

INTRODUCTION

Soft-shelled turtles (Trionychidae Bell, 1828) are a highly specialised clade of aquatic turtles, with 32 recognized extant species (Rhodin et al., 2021) and a rich fossil record (reviewed by Vitek and Joyce, 2015; Georgalis and Joyce, 2017). Members of the clade are easily distinguishable from other turtles by numerous apomorphies in the skull, shell, and other postcranial elements (e.g., Gaffney, 1979a; Meylan, 1987; Evers et al., 2022), including a flattened leathery carapace lacking keratinous scales and extensive temporal emarginations. This derived body plan has persisted since the Early Cretaceous (Li et al., 2015; Brinkman et al., 2017). Trionychid fossils are known from the Cretaceous of Asia, North America, and from one occurrence in Europe (Scheyer et al., 2012; Vitek and Joyce, 2015; Georgalis and Joyce, 2017). During the Palaeocene, trionychids were diverse and abundant in Asia, Europe, and North America, with sparse records from Australia and Africa (Vitek and Joyce, 2015; Georgalis and Joyce, 2017; Georgalis, 2021). Trionychid records from the Neogene include fossils from Europe, Asia, Africa, and North America, with sporadic occurrences from South America and Australia (Sánchez-Villagra et al., 2004; Head et al., 2006; Vitek and Joyce, 2015; Georgalis and Joyce, 2017).

Trionychidae, together with the family Carettochelyidae Gill, 1889, represented by the pig-nosed turtle *Carettochelys insculpta* Ramsay, 1887, as its sole living member, make up the superfamily Trionychia Baur, 1891 (e.g., Joyce et al., 2021). The family Trionychidae itself consists of two extant subfamilies (e.g., Joyce et al., 2021); Trionychinae Gray, 1825, which retains a poorly ossified carapace, and Cyclanorbinae Lydekker, 1889 (flap shell turtles), with secondary re-ossification of the carapace (e.g., Brinkman et al., 2017). The speciose fossil clade Plastomenidae Hay, 1902 (defined as the largest extinct clade containing *Plastomenus thomasii* Cope, 1872, sensu Joyce et al., 2021) is recovered as either stem-Cyclanorbinae (Joyce and Lyson, 2010, 2011; Li et al., 2015; Edgar et al., 2021; Jasinski et al., 2022; Evers et al., 2023) or stem-Trionychinae (Brinkman et al., 2017; Joyce et al., 2017). Alpha taxonomy and resolving even higher-level relationships between fossil trionychids is challenging as high homoplasy and interspecific variation in the clade make it difficult to define morphological characters.

The taxonomic history of Trionychidae is particularly convoluted. Since the historical revision of Trionychidae by Hummel (1929), numerous extant and fossil trionychid species have been synonymized and lead to the wastebasket genus *"Trionyx"* (e.g., Gaffney, 1979a; Meylan, 1987; Vitek and Joyce, 2015; Georgalis and Joyce, 2017). This was in large part due to a lack of a comprehensive and systematic interpretation of character variation (Meylan, 1987). Meylan (1987) performed the first phylogenetic analysis of extant trionychids based on osteological data. Consequently, he resurrected nine extant genera out of synonymy with *"Trionyx",* containing a total of 15 species. The phylogeny of extant trionychids has since been refined with the addition of molecular data (e.g., Engstrom et al., 2004; Le et al., 2014; Thomson et al., 2021), yet still many fossil specimens of uncertain placement are referred to as *"Trionyx",* and interrelationships of fossil trionychids remain contested (Vitek and Joyce, 2015; Georgalis and Joyce, 2017).

One such fossil trionychid genus with a convoluted history is *Axestemys* Hay, 1899, which currently includes seven species of large-bodied turtles dating from the Late Cretaceous (Campanian) to the Eocene (Lutetian) of North America and the Eocene (Ypresian) of Europe (Vitek, 2012; Vitek and Joyce, 2015; Georgalis and Joyce, 2017; Joyce et al., 2019). The genus has had multiple taxonomic revisions (e.g., Hutchison and Holroyd, 2003; Vitek, 2012; Vitek and Joyce, 2015). Of specific interest is *Axestemys infernalis* Joyce, Brinkman and Lyson, 2019, which includes all recorded *Axestemys* material from the Maastrichtian aged Lance and Hell Creek formations of the USA (Joyce et al., 2019). Members of the genus *Axestemys* have initially been recovered within crown-Trionychinae (Vitek, 2012). However, more recent analyses by Evers et al. (2023) place *A. infernalis* as either the sister taxon to crown-Cyclanorbinae or at the base of Pan-Cyclanorbinae. Specimens of *A. infernalis* are documented from nine localities across Montana, North Dakota, South Dakota, and Wyoming (Joyce et al., 2019). Joyce et al. (2019) noted loosely defined morphotypes based on shell material and two distinct 'end members', each related to a specific locality. Nonetheless, Joyce et al. (2019) argue there is sufficient overlap to justify grouping all material together into a single, yet highly variable, species.

The holotype of *Axestemys infernalis* is carapace DMNH 131100, whereas the authors purposefully refrained from assigning a cranium as holotype due to lack of diagnostic features. The presence of cranial sculpturing has been proposed as a diagnostic feature of the genus (Vitek and Joyce, 2015; Georgalis and Joyce, 2017), but two

additional documented specimens of *A. infernalis* display a completely smooth skull roof (Joyce et al., 2019). Current diagnostic characters of both the genus *Axestemys* and *A. infernalis* are based solely on the carapace (Joyce et al., 2019). The three published cranial specimens of *A. infernalis* are associated with postcranial material, known from North- and South Dakota: DMNH 98814 (previously assigned to *Axestemys splendidus* Hay, 1908 [Vitek, 2012, therein MRF 266]), DMNH 130951, and NSM PV24650 (Joyce et al., 2019). Herein we present a new isolated cranium of *A. infernalis*, MAB13742 (Figure 1), from the Lance Formation of Niobrara County, Wyoming. This specimen represents the first documented trionychid skull of the Lance Formation of Wyoming. Moreover, we discuss interspecific variation in the cranium of *A. infernalis* and compare it to crania of other *Axestemys* species. Finally, we update the character matrix of Evers et al. (2023) to present new phylogenetic hypotheses of Trionychia.

Institutional Abbreviations

AMNH = American Museum of Natural History, New York, New York, USA; BMNH = British Museum of Natural History (Natural History Museum), London, UK; DMNH = Denver Museum of Nature and Science, Denver, Colorado, USA; FMNH = Field Museum of Natural History, Chicago, Illinois, USA; IW = Ingmar Werneburg Private Collection; MAB = Oertijdmuseum, Boxtel, Netherlands; MRF = Marmarth Research Foundation, Marmarth, North Dakota, USA; NSM = National Museum of Nature and Science, Tokyo, Japan; UMMP = University of Michigan Museum of Paleontology, Ann Arbor, Michigan, USA.

Data Availability Statement

The raw scan files are made available at MorphoSource Media ID: 000635277.

MATERIAL AND METHODS

MAB13742 was recovered near Lusk in Niobrara County, Wyoming, USA. The exact location will not be disclosed due to the vulnerability of the locality. The collection site is an outcrop of thick-bedded buff sandstone at the base of the Lance Formation 4 m underneath a small microfossil site. The well-sorted grains are poorly cemented result-

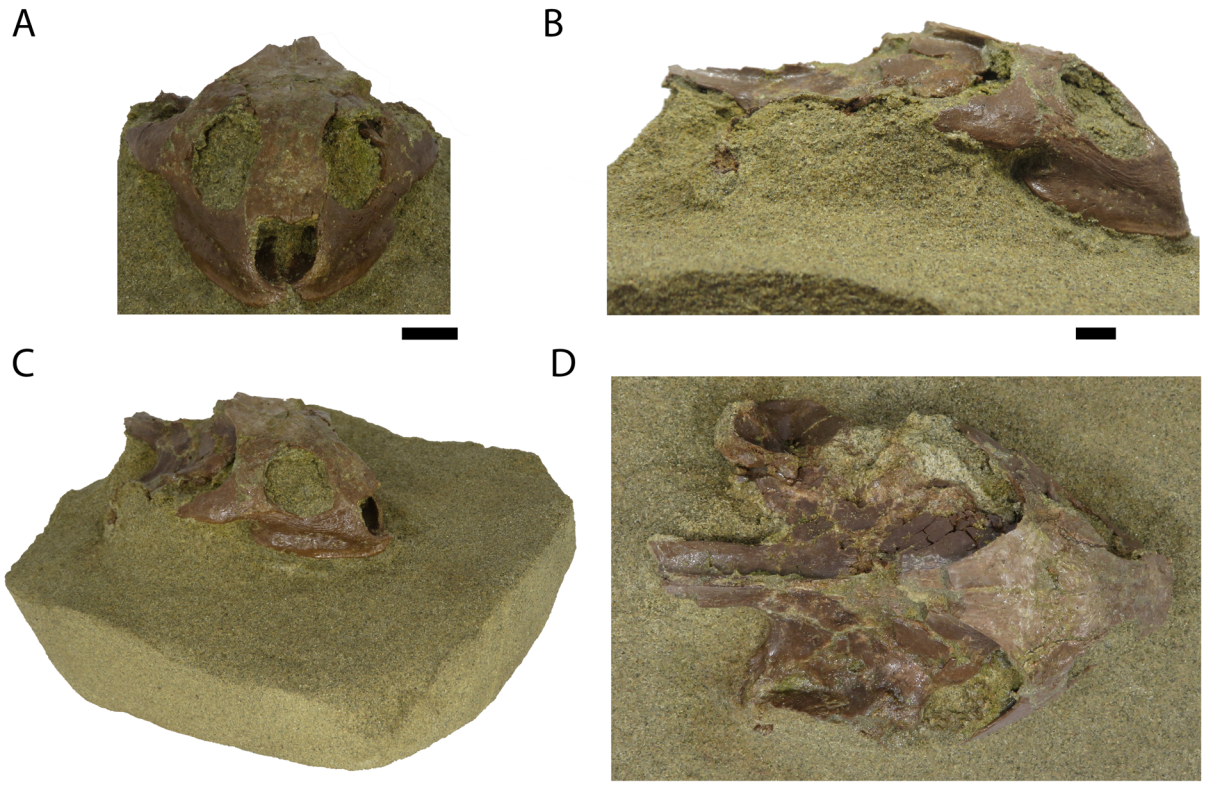

FIGURE 1. Photographs of the cranium of *Axestemys infernalis* MAB13742 embedded in matrix. A anterior view, B right lateral view, C oblique overview, D dorsal view. Both scale bars equal 1 cm; scale bar A applies to the anterior view; scale bar B applies to both right lateral and dorsal view.

ing in a soft rock that is unstratified. Overall, the natural erosion surface of this strata is not remarkably fossiliferous.

The specimen was mechanically prepared at the Oertijdmuseum in Boxtel, Netherlands, by one of us (JJWW), prior to description. Because of the fragile nature of the specimen and loose sediments, as well as aesthetic value, it was decided to keep the cranium partly embedded in the sandstone matrix (Figure 1).

To study the palatal anatomy, the specimen was scanned at Jeroen Bosch Ziekenhuis in 's Hertogenbosch, Netherlands, with a Siemens Somatom Definition Flash medical CT scanner. The scan was performed at 1400 µA and 120 kV, resulting in a voxel size of 51.3 µm. The scan was visualised using VGStudio Max v3.3.

We update herein the most recent trionychian character matrix of Evers et al. (2023). This matrix resulted from a number of iterations since the inaugural paper on trionychian systematics by Meylan (1987), which includes only extant species. Meylan (1987) acknowledged the high number of interspecific variation in Trionychia, and included "two-state characters in which both states frequently occur in the same species, requiring the recognition of that third, intermediate condition" (Meylan, 1987, p. 8), or frequency-based coding (e.g., Smith and Gutberlet 2001). This type of coding is problematic, especially in the context of fossil taxa with limited material available and/or spanning large temporal and palaeogeographical scales. Although Evers et al. (2023) updated the previously most recent character matrix of Lyson et al. (2021) to, amongst other changes, rephrase frequency-based characters to polymorphic characters, this was not reflected in either their list of characters nor was it mentioned in their manuscript. We follow Evers et al. (2023) and retain these characters as polymorphic. In addition, the following scores of *Axestemys infernalis* are updated based on our observations of MAB13742: ch. 31: 1 -> 1 and 2; ch. 44: 1 -> 2; ch. 99: ? -> 2. These changes reflect interspecific variation in *A. infernalis* (character 31 and character 44) and previously undocumented anatomical information (character 99). Lastly, we fix a coding error for character 33 pertaining a basisphenoid-palatine contact in Evers et al. (2023). Absence (state 1) is scored correctly in the outgroup *Adocus* (Meylan and Gaffney, 1989), while it is present (state 2) in *Carettochelys insculpta* (e.g., Walther, 1922). However, for the remaining extant taxa the coding is likely swapped. Absence of a basisphenoid-palatine contact is diagnostic for *Rafetus euphraticus* Daudin, 1802 among extant trionychids (Meylan 1987), yet the matrix of Evers et al. (2023) codes this character as present in *R. euphraticus* and absent in all other extant trionychids. Similarly, a basisphenoid-palatine contact is present in the fossil taxon *Gobiapalone orlovi* Khosatzky, 1976 MPC 25/160 (Danilov et al., 2014), but it is scored as absent in the matrix of Evers et al. (2023). The changes to the character scores are summarized in Appendix 1. In addition, we include our final list of characters (Appendix 2) and character matrix (Appendix 3).

Following Evers et al. (2023), we ran both a parsimony analysis and a Bayesian analysis. In both analyses, the relationships of extant trionychians were forced into following the molecular phylogeny of Thomson et al. (2021), after which fossil taxa were added. Consequently, character 27 (pertaining sexual dimorphism in disc length) is rendered non-informative as it was not applicable to any of the fossil taxa included. This character is retained nonetheless, as future analyses may incorporate trionychian taxa for which this character can be scored. Additionally, *Adocus lineolatus* Cope, 1874 was assigned as the outgroup. Characters 1, 3, 5, 16, 18–20, 22, 31, 40, 44, 53–54, 59, 77, 102, and 108–110 describe morphoclines and were thus ordered.

The parsimony analysis was ran in TNT 1.5 (Goloboff and Catalano, 2016). We followed the same steps as Evers et al. (2023) – using a New Technology Search with initial level set to 30, finding the minimum length 30 times and enabling all tree search functions. We performed the analysis only once, with an implied weighting constant of K = 12, as this method outperformed the equal weighting analysis in Evers et al. (2023). Lastly, we ran an updated version of the script Evers et al. (2023) wrote for MrBayes 3.2.6 (Ronquist et al., 2009), updating character scores as discussed above (Appendix 4).

SYSTEMATIC PALAEONTOLOGY

TESTUDINATA Klein, 1760
CRYPTODIRA Cope, 1868
Superfamily TRIONYCHIA Baur, 1891
Family TRIONYCHIDAE Bell, 1828
Genus *AXESTEMYS* Hay, 1899
Axestemys infernalis Joyce, Brinkman and Lyson, 2019
Figures 1–8

.2012 *Axestemys splendida* Hay; Vitek, p. 16, pl. 8, p. 17, pl. 9, figs 1, 2, 3, 4

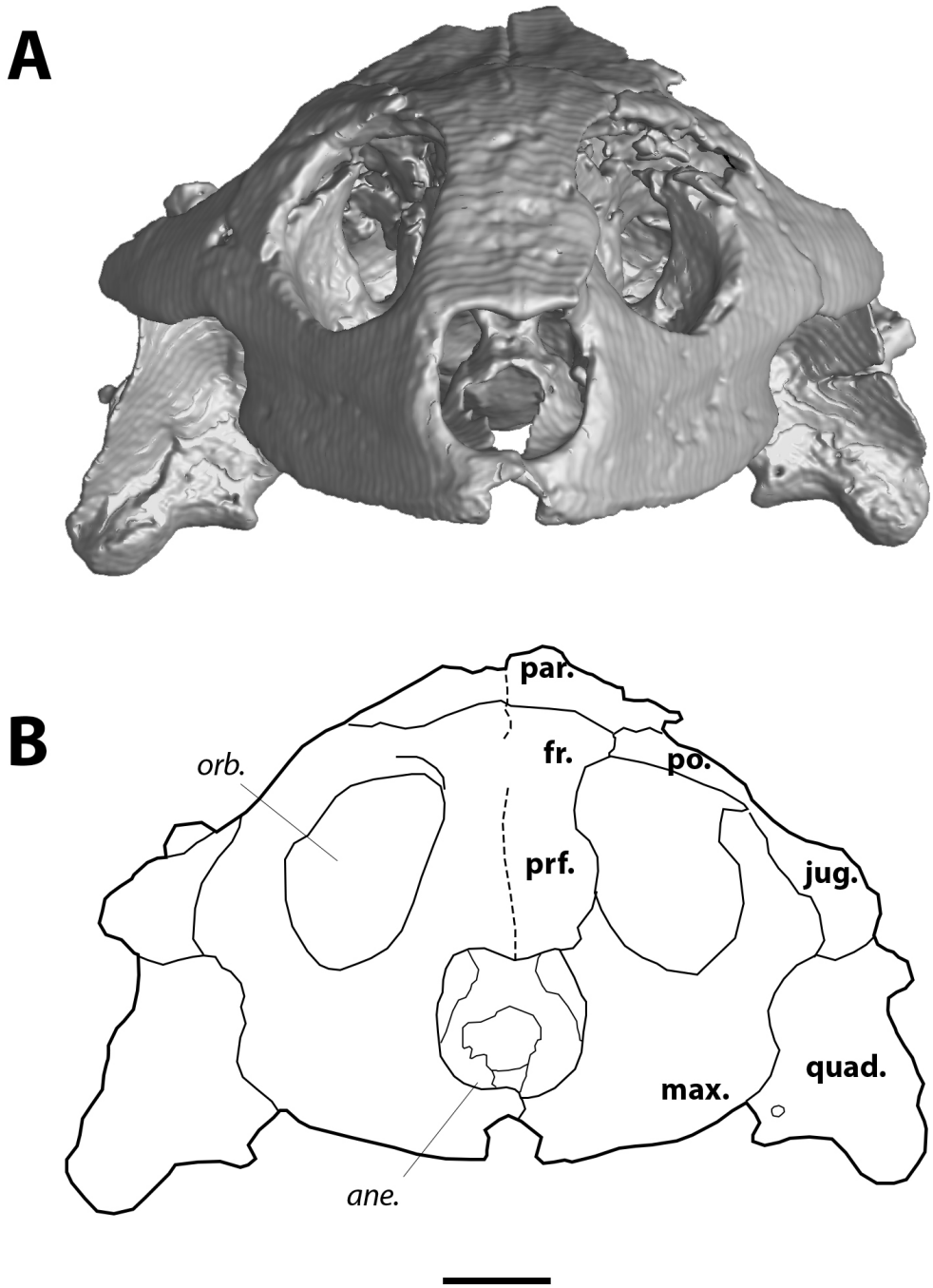

FIGURE 2. Reconstruction of the cranium of *Axestemys infernalis* MAB13742 in anterior view. A shows the digital rendering of the CT-scan and B the interpretative line drawing. Dashed lines are observed sutures, dotted lines indicate damage. Scale bar equals 1 cm. Abbreviations: *ane.* apertura narium externum, *orb.* orbit, **fr.** frontal, **jug.** jugal, **max.** maxilla, **par.** parietal, **po.** postorbital, **prf.** prefrontal, **quad.** quadrate.

Taxonomic Assignment

MAB13742 resembles the three other known skulls of *Axestemys infernalis* in having blunt and deep maxillae, triturating surfaces that do not form a secondary palate, and a postorbital that extends over the entire anteroposterior length of the postorbital bar. These traits are also present in the other species of *Axestemys* with well-preserved crania; *Axestemys splendida* (TMP 90.59.01 and UALVP 5000) from the Campanian of Montana (Gardner et

al. 1995), *A. montinsana* Vitek, 2012 (UMMP 27029) from the Palaeocene of Montana (Vitek, 2012) and *A. vittata* Pomel, 1847 (BMNH R8694) from the Eocene of England (Walker and Moody, 1985, therein *Eurycephalochelys fowleri*). We thus assign MAB13742 to *A. infernalis*, following the assignment of all Lance and Hell Creek material of *Axestemys* to *A. infernalis* by Joyce et al. (2019).

Overall Preservation

MAB13742 comprises a relatively complete skull. The bones of the skull roof are fairly smooth (Figure 1), in contrast to the sculptured skull roof in NSM PV24650 (Joyce et al., 2019). Although the skull surface appears ribbed on the scan images (Figures 2-7), this is an artefact of the scan. Overall, the right half of MAB13742 is better preserved, and lies slightly anterior to the left half. The posterodorsal region is poorly preserved. Notably, the posterodorsal portion of the crista supraoccipitalis is broken off. The dorsal surface of the processus trochlearis oticum bears various cracks, so that bone contacts are not discernible. Both zygomatic arches are broken posteriorly. The basioccipital, squamosal, and quadratojugal are either missing or severely damaged.

Overall Proportions

Although MAB13742 is relatively large (snout – occipital condyle length 9.8 cm [occipital condyle is missing, measured snout – midline of quadrate condyles]), it is significantly smaller than DMNH 98814 (14.5 cm), the smallest skull reported by Joyce et al. (2019). As in trionychids (Gaffney, 1979b), the temporal emargination is well-developed. The anterior portion of the skull is roughly triangular in outline (Figure 3). The orbits are large, roughly two-thirds of the skull in dorsoventral height, and appear to project anteriorly (Figures 2, 4).

Osteology

The prefrontal is the anteriormost bone of the skull roof, comprising the dorsal margin of the apertura narium externum and the anteromedial wall of the orbit (Figures 2, 3). The apertura narium externum is weakly excavated laterally to a similar degree as DMNH 98814 (Vitek, 2012), but it is not as extensive as in DMNH 130951 (Joyce et al., 2019). Both prefrontals suture at the midline, which is discernible as a straight line through most of its course. The prefrontal contacts the maxilla anteroventrally, anterior to the orbit, yet seems to be fused to the frontal dorsally. Through a descending process, it contacts the dorsal side of the vomer within the orbit.

The frontal continues roofing the orbit and includes the dorsalmost point of the orbit (Figures 2, 3). Similar to the prefrontals, the frontals meet along a straight suture at their midline. In dorsal view, the frontal sutures with the parietal halfway the postorbital bar and contacts the anterodorsal portion of the postorbital. The anteroventral suture with the prefrontal is not visible.

Only a small portion of the parietals is preserved, as the anteromedial margin of the temporal emargination and the anteromedial portion of the processus trochlearis (Figure 3). On the skull roof, the parietals are slightly depressed safe for a modest ridge that defines their medial suture. The parietal forms a straight suture with the frontal anteriorly and with the postorbital anterolaterally. On the processus trochlearis, it has a lateral contact with the prootic. The posterior portion of the parietal, that would have contributed to the crista supraoccipitalis, is broken off.

The postorbital forms both the posterior margin of the orbit and the anterior margin of the temporal emargination (Figures 3, 4). It extends ventrally to near the ventral margin of the orbit, contacting the maxilla ventrally and overlying the jugal – thus excluding the jugal superficially from the orbit. Expansion of the bone makes up most of the postorbital bar in lateral view, forming the dorsal most two-thirds of the posterior margin of the orbit. The lateral exposure of the postorbital is thereby much greater than in DMNH 130951 (Joyce et al., 2019, figure 18) and the other known crania of *Axestemys* (Walker and Moody, 1985; Vitek, 2012). Dorsally, the postorbital forms a broad contact with the frontal anteriorly and the parietal posteriorly. The lateral surface of the postorbital features some shallow anteroventral-posterodorsal oriented grooves.

The jugal is present as a tall but mediolaterally thin bone along the anterolateral margin of the skull and comprises part of the zygomatic arch (Figures 3, 4). Anteriorly, it is overlain by the postorbital dorsally and a posterior process of the maxilla ventrally. This configuration causes a superficial exclusion of the jugal to the orbit in lateral view unlike the other specimens of *Axestemys infernalis* (Vitek, 2012; Joyce et al., 2019). Whether the jugal continues anteriorly underneath the maxilla and postorbital to reach the orbit could not be determined. Only the anterior portion of the zygomatic arch is preserved, so its relation to either the

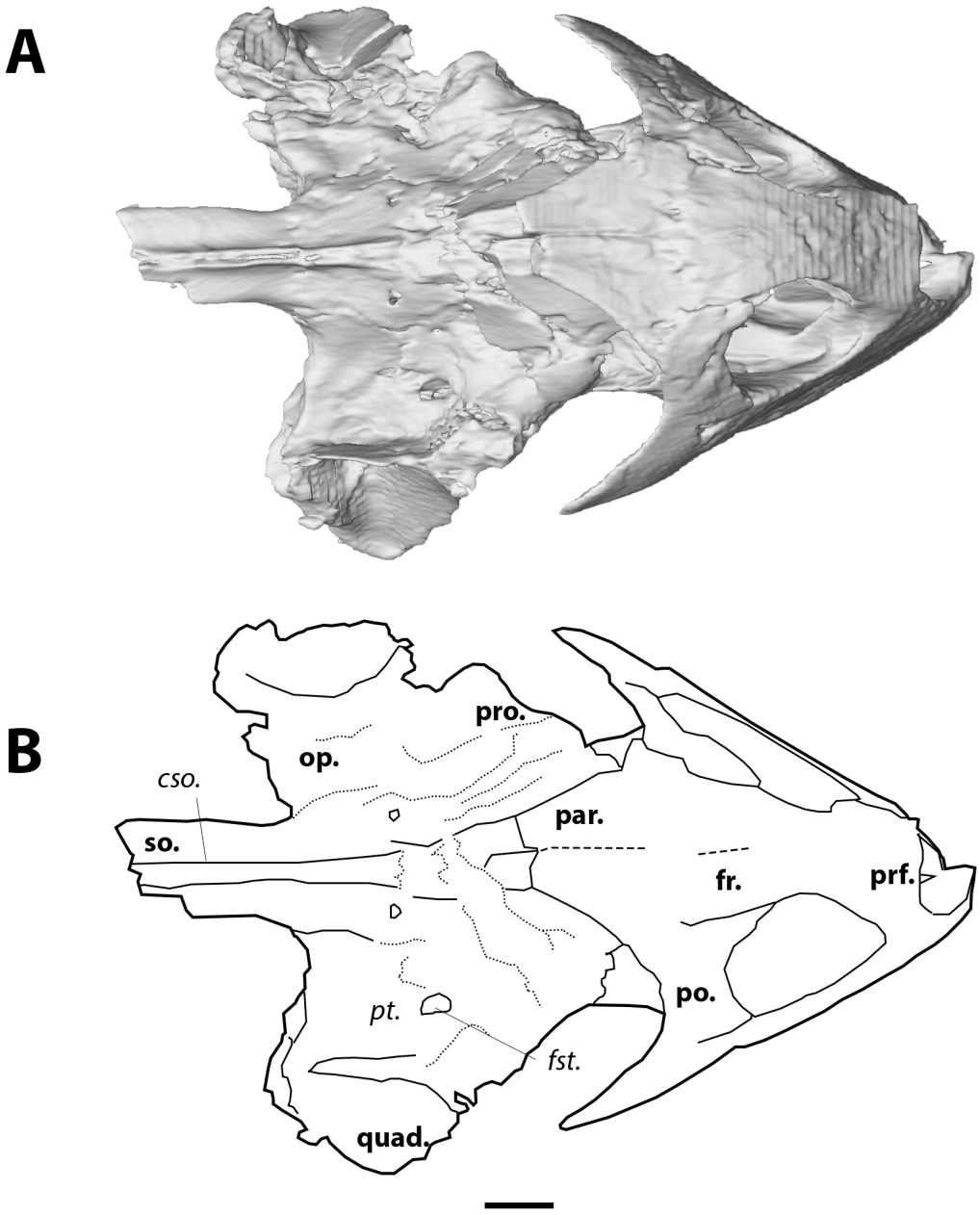

FIGURE 3. Reconstruction of the cranium of *Axestemys infernalis* MAB13742 in dorsal view. A shows the digital rendering of the CT-scan and B the interpretative line drawing. Dashed lines are observed sutures, dotted lines indicate damage. Scale bar equals 1 cm. Abbreviations: *cso.* crista supraoccipitalis, *fst.* foramen stapedio-temporale, *pt.* processus trochlearis, **fr.** frontal, **jug.** jugal, **par.** parietal, **po.** postorbital, **prf.** prefrontal, **pro.** prootic, **quad.** quadrate, **so.** supraoccipital.

quadratojugal, squamosal, or pterygoid are unknown.

The presence of the quadratojugal in MAB13742 is uncertain, as the posterior portions of the zygomatic arches are missing, and the dorsal surface of the quadrates is damaged. If the quadratojugal is present, it is merely by small fragments that do not yield useful morphological information.

The squamosal is likely missing or at least severely broken. In other *Axestemys infernalis* specimens, the squamosal forms an elongate posterior process that extends beyond the occipital condyle (Joyce et al., 2019). No such structure is preserved in MAB13742. Potential areas of con-

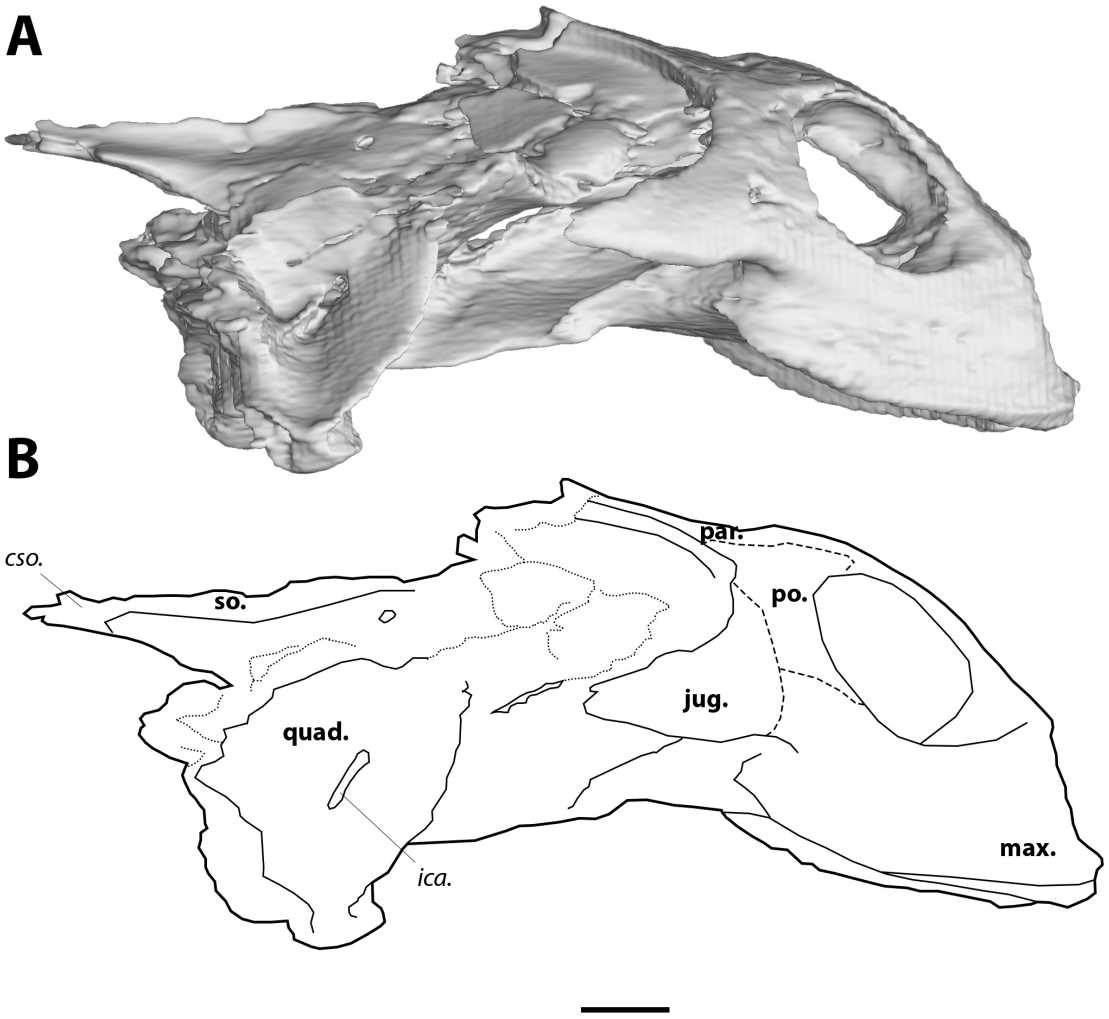

FIGURE 4. Reconstruction of the cranium of *Axestemys infernalis* MAB13742 in right lateral view. A shows the digital rendering of the CT-scan and B the interpretative line drawing. Dashed lines are observed sutures, dotted lines indicate damage. Scale bar equals 1 cm. Abbreviations: *cso.* crista supraoccipitalis, *ica.* incisura columellae auris, **jug.** jugal, **max.** maxilla, **par.** parietal, **po.** postorbital, **quad.** quadrate, **so.** supraoccipital.

tact, such as the dorsal portion of the quadrate and the posterior portion of the quadratojugal are also missing or damaged.

There is no ossified premaxilla present in MAB13742 (Figure 2). This bone is present and ossified in DMNH 98814 and NSM PV24650 (Joyce et al., 2019), and the known crania of *Axestemys splendida* (Gardner et al. 1995), *A. montinsana* (Vitek, 2012), and *A. vittata* (Moody and Walker, 1970; Walker and Moody, 1985).

The maxilla is a dorsoventral deep bone that composes the entire ventral margin of orbit, as well as the lateral and ventral wall of apertura narium externum (Figures 2, 4). In anterior view the maxillae form an arch ventral to the apertura narium externum, a consequence of the absence of the premaxilla. Inside the nasal capsule, the medial side of the maxilla bears a posteriorly oriented supraalveolar foramen (Figure 5). The maxilla contacts the prefrontal anteriorly to the orbit along a straight suture. In contrast to other *Axestemys infernalis* specimens, where the maxilla-jugal contact is positioned ventral to the orbit (Vitek, 2012; Joyce et al., 2019), in MAB13742 the maxilla-jugal is achieved posteroventral to the orbit by a posterior process of the maxilla. This process overlies the jugal and contacts the postorbital posterodorsally. The slightly concave lateral surface is pitted and few shallow anteroposteriorly oriented grooves stretch, ventral to the orbit, from its anterior margin

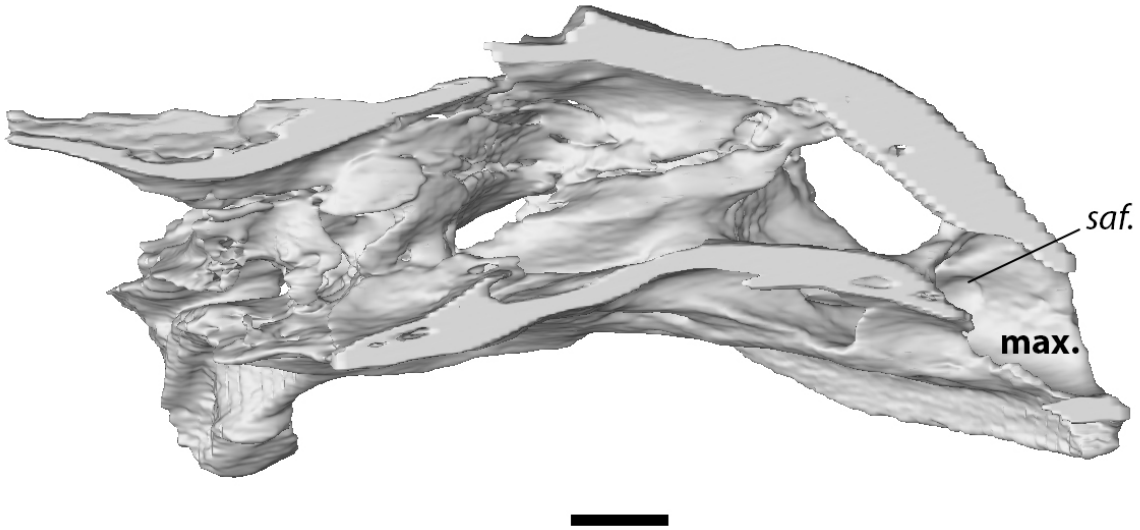

FIGURE 5. Reconstruction of the cranium of *Axestemys infernalis* MAB13742, digital rendering of the CT-scan showing the internal view of right lateral side and the supraalveolar foramen of the maxilla. Scale bar equals 1 cm. Abbreviations: *saf.* supraalveolar foramen, **max.** maxilla. Mirrored.

to the posterior process of the maxilla. The ventral margin of the maxilla curves gently posterodorsally in lateral view. Ventrally the maxilla forms a moderately wide, flat, triturating surface that is pitted with foramina (Figure 6). These triturating surfaces do not meet at the midline, so that the vomer remains exposed. The triturating surfaces lack a prominent lingual margin, instead terminating in a modestly rounded edge. Sutures on the ventral side are not discernible, so its contribution to the foramen palatinum posterius could not be assessed.

In ventral view, the vomer is visible between the triturating surfaces of the maxillae (Figure 6). Anteroventrally, it has a broad concave surface, its dorsal most point midway, which forms the anterior portion of the internal nares. The vomer bears a mediolaterally thin posterior process that extends one third into the anteroposterior length of the palatines. A thin groove runs along the midline of this process. Further posterior, a low ridge continues the trajectory of this process until the dorsal margin of the internal nares, but it is unclear whether this is a continuation of the vomer or merely in between the palatines. The vomer contacts the maxilla anterolaterally, the descending process of the prefrontal anterodorsally, and the palatines posterodorsally. Due to the resolution of the scan, the presence of foramina such as the praepalatine foramina, is unclear.

The palatine is a sheet-like bone that floors the nasal canal (Figure 6). In ventral view, it forms the posterior part of the internal nares and lies further dorsal to the triturating surfaces and the vomer. A ridge runs along its midline, but it is unclear whether this ridge is an extension of the posterior process of the vomer or is formed by the palatines themselves. It contacts the vomer ventrally and reaches the parietals on the skull roof through an ascending process. Laterally, it contacts the maxillae, but the precise suture between the palatine and the maxilla is not visible. Posteriorly it contacts the pterygoid, but the precise location of this suture, as well as a potential contact with the basisphenoid, is unclear.

The pterygoid forms a major part of the posteroventral side of the cranium (Figure 6). Its lateral margin is characterised by a slight ventrally curved ridge, and a lateral flange is absent. Posteriorly, at the level of the base of the foramen magnum, the pterygoid bears the opening of the foramen posterius canalis carotici interni (Figure 7). Posteromedially, the pterygoid wraps around the basisphenoid, and it contacts the quadrate posterolaterally. The anterior sutures of the pterygoid are not visible, nor is it clear whether the pterygoids have a midline contact anteriorly to the basisphenoid.

Joyce et al. (2019) could not assess the presence of an epipterygoid due to the crushed trigeminal region in all three available specimens. Unfortunately, its presence in MAB13742 is similarly unclear due to preservation.

The quadrate is recognisable as a roughly triangular bone at the posterolateral side of the cranium, that forms the deep cavum tympani and

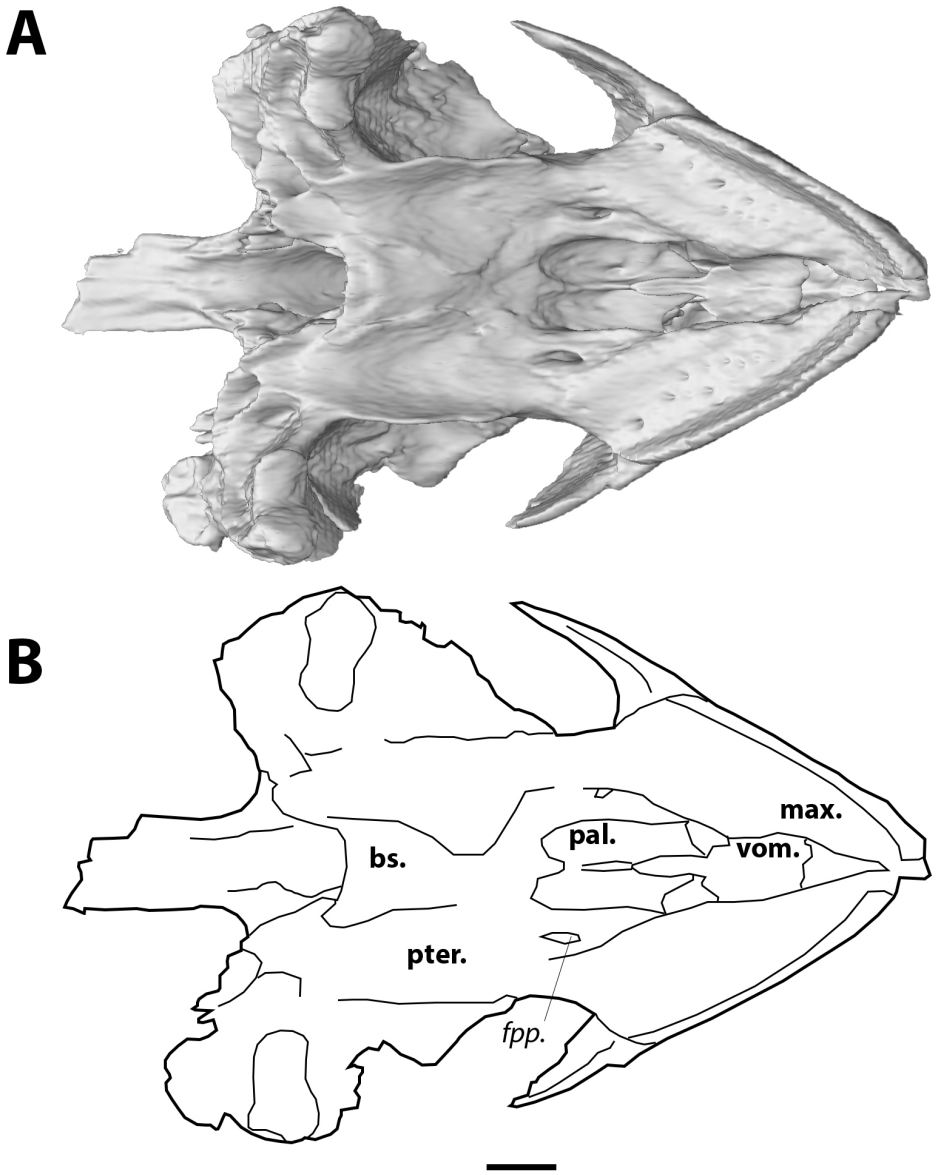

FIGURE 6. Reconstruction of the cranium of *Axestemys infernalis* MAB13742 in ventral view. A shows the digital rendering of the CT-scan and B the interpretative line drawing. Scale bar equals 1 cm. Abbreviations: *fpp.* foramen palatinum posterius, **bs.** basisphenoid, **max.** maxilla, **pal.** palatine, **pter.** pterygoid, **vom.** vomer.

houses the incisura columellae auris (Figure 4). This bone sits relatively far posteriorly, further than the foramen stapedio-temporale. Ventrally, the quadrate forms the bipartite articular condyle, posterior to the basisphenoid (Figure 6). The lateral facet of the articular condyle is slightly more anteroposteriorly elongate and deeper than the medial facet. While it is clear the quadrate has a broad dorsal contact with the processus trochlearis, the exact sutures are not discernible.

The prootic borders the anterior margin of the processus trochlearis (Figure 3). It has a medial contact with the parietal. The lateral margin, where it would have contacted the anterior portion of the quadrate, is broken off. Moreover, as the dorsal surface of the processus trochlearis is shattered, the distal sutures of the prootic are not discernible. Nonetheless, the foramen stapedio-temporale remains visible, and is roughly triangular in shape.

The opisthotic sits at the posterior side of the processus trochlearis. It is visible in dorsal and

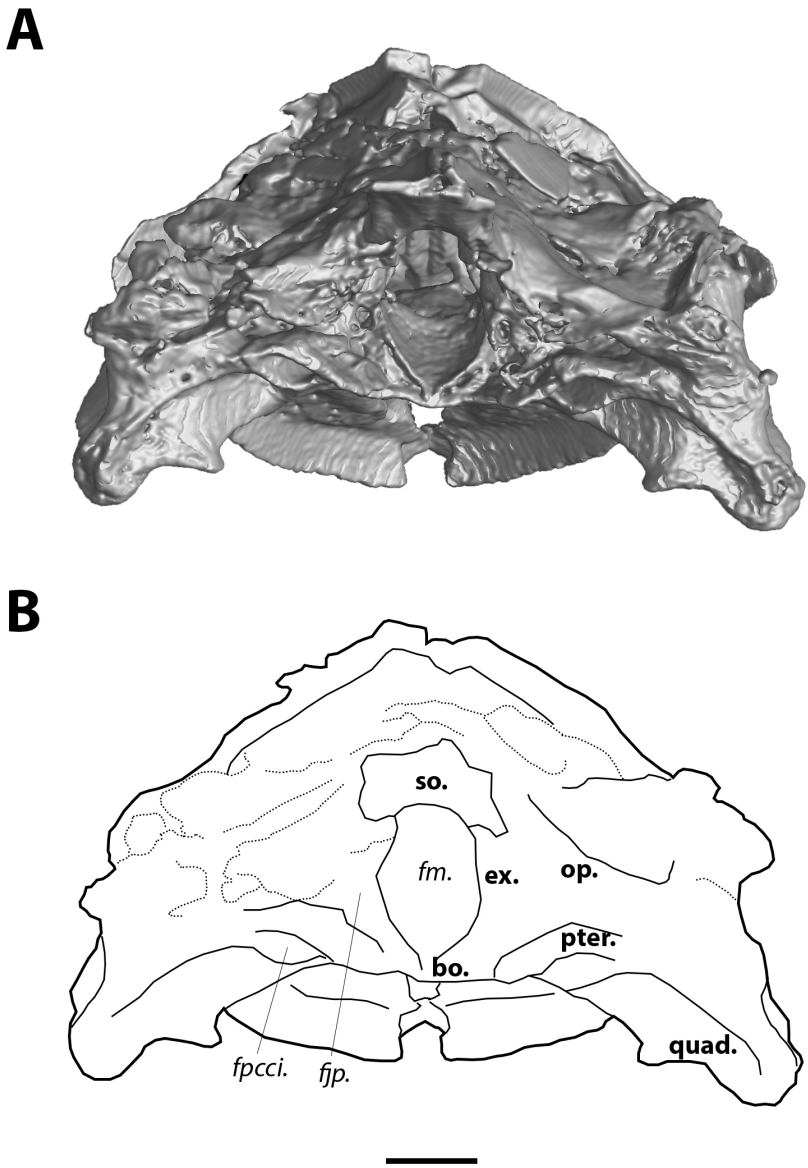

FIGURE 7. Reconstruction of the cranium of *Axestemys infernalis* MAB13742 in posterior view. A shows the digital rendering of the CT-scan and B the interpretative line drawing. Scale bar equals 1 cm. Abbreviations: *fjp.* foramen jugulare posterius, *fm.* foramen magnum, *fpcci.* foramen posterius canalis carotici interni, **ex.** exoccipital, **op.** opisthotic, **pter.** pterygoid, **quad.** quadrate, **so.** supraoccipital.

occipital views (Figures 3, 7), but due to the fragmentary nature of the dorsal side of this process, its sutures are not discernible.

The supraoccipital forms posterodorsal portion of skull, and roofs the foramen magnum (Figures 3, 4). The crista supraoccipitalis is mostly broken off, yet the supraoccipital still forms the posterior most portion of the cranium of MAB13742. Anterolaterally, the supraoccipital bears two seemingly symmetrical depressions, which are more apparent on the CT rendering than on the actual specimen (Figure 3). Both depressions are the result of damage.

The exoccipital forms the lateral wall of the foramen magnum and is visible in occipital view (Figure 7). It bears the small foramen jugulare posterius, but no further details could be inferred about the shape and contacts of the exoccipital in MAB13742.

The basioccipital is not preserved in MAB13742.

The foramen magnum is floored by the basisphenoid (Figure 7). The basisphenoid is a relatively small, triangular-shaped unpaired element visible at the posteroventral side of the palate. It connects to the pterygoids laterally, but it is unclear whether its anterior margin sutures to the pterygoids or the palatines.

Neuroanatomy

The neuroanatomy has not been described for any *Axestemys* species yet. Few studies considered variation in the morphology of the turtle brain endocast using geometric morphometrics (Lautenschlager et al., 2018; Ferreira et al., 2022) but found little differentiation between adults of major extant clades. No trionychid braincase endocast has been described in detail. Here we compare the braincase endocast with that of the extant trionychine trionychids *Apalone spinifera emoryi* Agassiz, 1857 FMNH 21178 and *Pelodiscus sinensis* Wiegmann, 1835 IW576-2 (Werneburg et al., 2021a). The resolution of the scan of MAB13742 unfortunately did not permit individual segmentation of the semicircular canals, instead showing the endosseous labyrinth as an undifferentiated single cavity. However, general statements about its proportions can be made. The endosseous labyrinth of MAB13742 is compared to the described endosseous labyrinth of the plastomenid *Plastomenus thomasii* AMNH FR 6015 (Evers et al., 2023), and to the extant trionychids *Apalone spinifera emoryi* FMNH 21178 (Media ID 00037651, Ferreira et al., 2021), *Amyda cartiliginea* Boddaert, 1770 FMNH 244117 (Media ID 000372714, Evers, 2021) and *P. sinensis* IW576-2 (Media ID 000373752; Evers, 2021) that were available on MorphoSource. Additionally, the carotid artery and facial nerve canal systems could not be segmented.

Overall, the braincase endocast of MAB13742 is anteroposteriorly elongate and tubular (Figure 8). As in other turtles (Ferreira et al., 2022), there is no clearly defined boundary between the braincase endocast and nasal cavity in MAB13742 (Figure 8B). In all three specimens, the cerebral region is the most transversely wide. In *Apalone spinifera emoryi* and *Pelodiscus sinensis,* the width decreases gradually anteriorly towards the sulcus olfactorius, giving it roughly an arrowhead shape in dorsal view. In *Axestemys infernalis*, on the other hand, the decrease in width is more pronounced posteriorly than anteriorly, so that the area directly posterior to the sulcus olfactorius is medially constricted (Figure 8A). Moreover, paired spike-like projections are present ventrally at the posterior portion of the sulcus olfactorius in *A. infernalis* (Figure 8C) as in *P. sinensis*, which are missing in *A. spinifera*. In all three turtles, the optic and cerebellar region is medially constricted to make room for the endosseous labyrinth. This region widens posteriorly, but the widening is more pronounced in *A. infernalis* than in *A. spinifera* and *P. sinensis*. MAB13742 bears an elongate ‘cartilaginous rider’ (Figure 8B), similar to what Werneburg et al. (2021b) observed in the extant trionychids *A. spinifera* and *P. sinensis*. In lateral view, the sulcus olfactorius is more dorsoventrally tall in *A. infernalis* than *A. spinifera* and *P. sinensis*. The entire braincase endocast is oriented horizontally in *P. sinensis*, while the sulcus olfactorius is deflected dorsally in MAB13742 and in *A. spinifera*. Ventrally, the endocast of the pituitary fossa of MAB13742 forms a relatively wide cone that is directed anteriorly (Figure 8C), and is much more pronounced than in *A. spinifera*, while this structure is rectangular in *P. sinensis.*

The foramen ovalis is relatively extensive ventrally in MAB13742 (Figure 8B) compared to the extant trionychids as it is deeper than the semicircular canals; in *Plastomenus thomasii* AMNH FR 6015 the foramen ovalis was damaged so that its ventral extend could not be determined (Evers et al., 2023). Moreover, the foramen ovalis in MAB13742 curves lateroventrally, so that it is visible from dorsal view (Figure 8A), unlike in the other trionychians. In MAB13742, the cavity for the anterior semicircular canal is significantly farther extended anteriorly than the posterior semicircular canal is extended posteriorly, as in *P. thomasii* (Evers et al., 2023). The depression of the common crus is minor and the dorsal most point of both the anterior and posterior semicircular are roughly at the same level, while the anterior semicircular canal is clearly more dorsally expanded in the other trionychians (Figure 8B).

Phylogeny

The parsimony analysis under K = 12 yielded three trees with a score of 15.94107, which is slightly lower than the score of 15.97 reported by Evers et al. (2023). Figure 9A shows the strict-consensus topology of these three trees, which is overall similar to the topology of the parsimony analysis of Evers et al. (2023). Similar to their analysis, *Axestemys infernalis* is placed as the sister-taxon to a clade composed of (Cyclanorbinae + *Helopanoplia distincta* Hay, 1902) + Plastomenidae (Figure 9A). By contrast, *A. infernalis* does not represent the earliest branch of Pan-Cyclanorbinae in

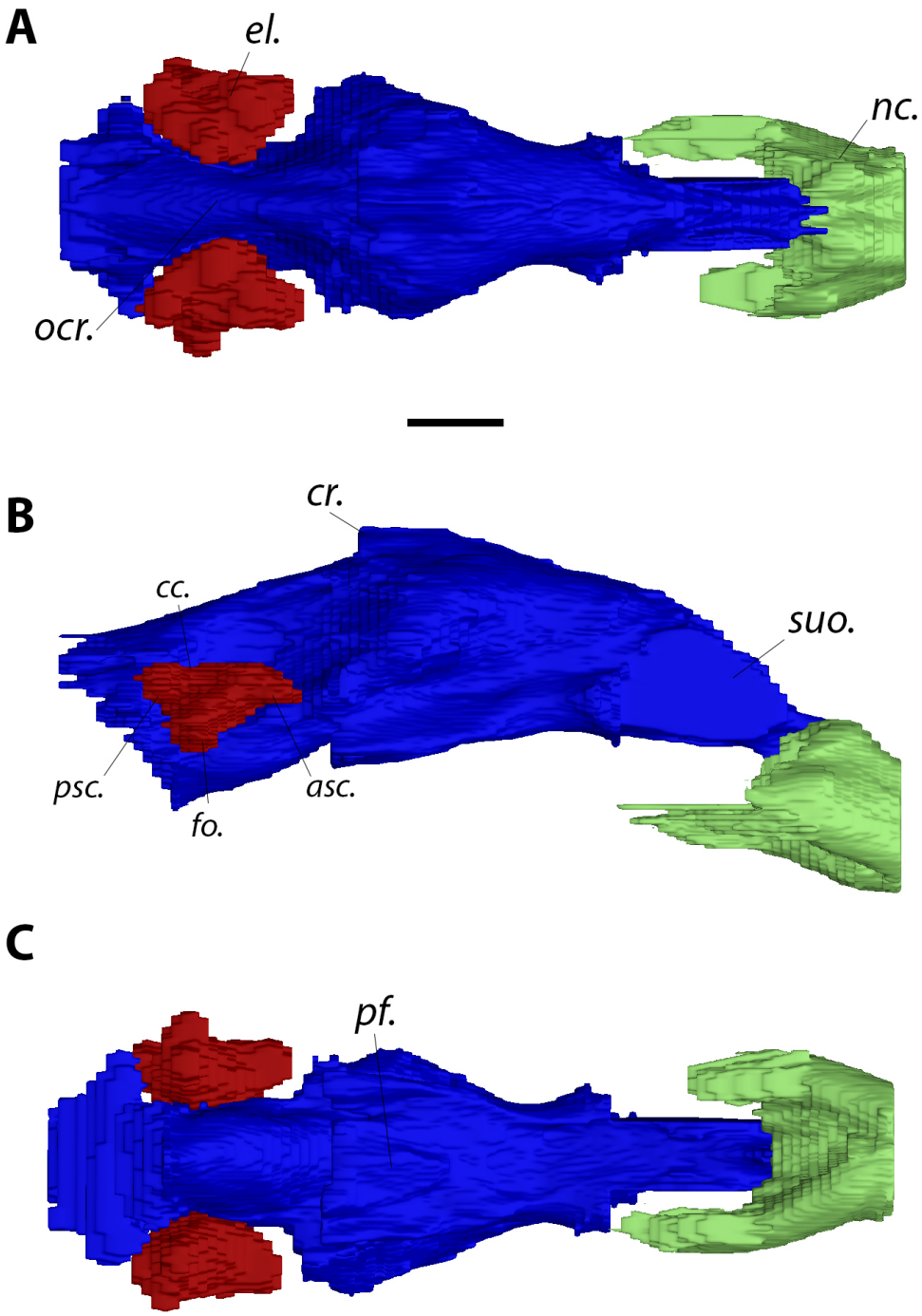

FIGURE 8. Digital reconstruction of the braincase endocast of *Axestemys infernalis* MAB13742 in A dorsal, B right lateral and C ventral views. Scale bar equals 1 cm. Abbreviations: *acs.* anterior semicircular canal, *cc.* common crus, *cr.* cartilaginous rider, *el.* endosseous labyrinth, *fo.* foramen ovalis, *nc.* nasal cavity, *ocr.* optic and cerebellar region, *pf.* pituitary foramen, *pcs.* posterior semicircular canal, *suo.* sulcus olfactorius.

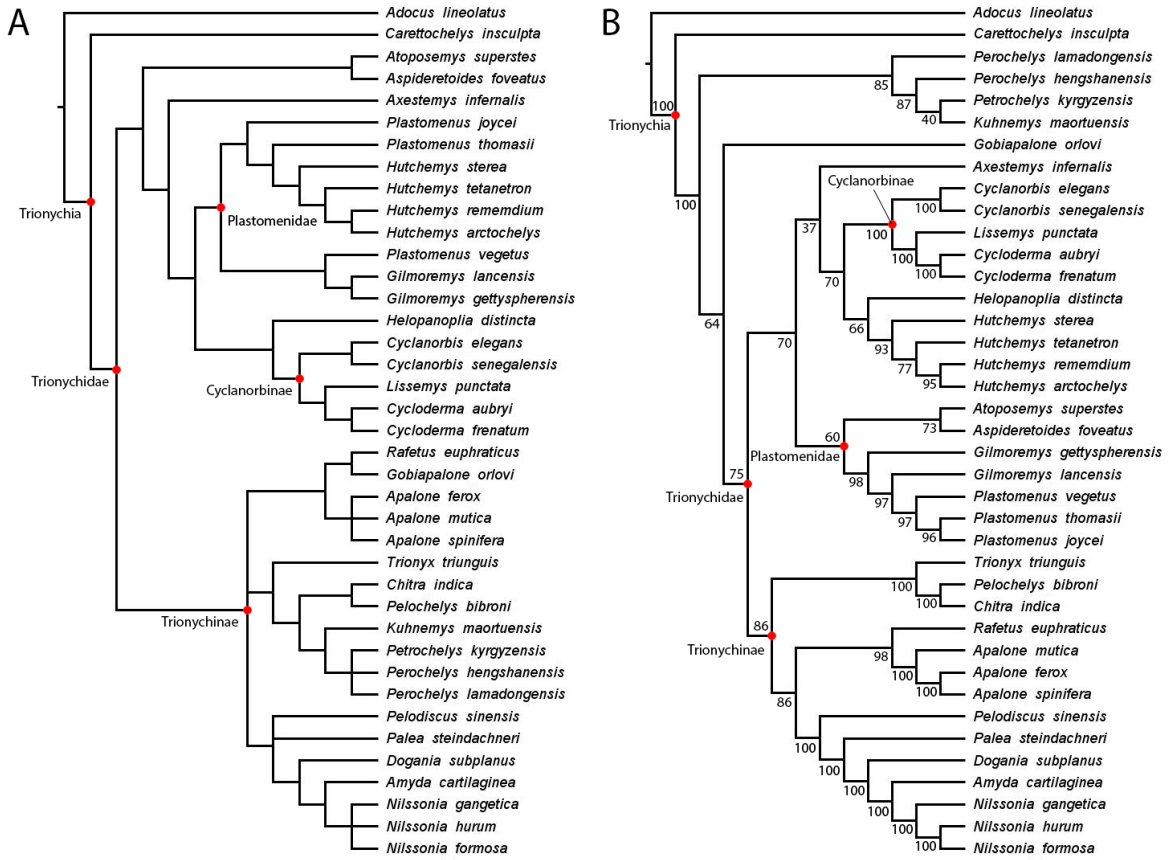

FIGURE 9. Cladograms showing A the results of the parsimony analysis in TNT, using a concavity constant of K = 12. B shows the results of the Bayesian analysis. Support values are indicated for each node.

our analysis. We recover the clade *Atoposemys superstes* Russell, 1930 + *Asipederetoides foveatus* Gardner et al., 1995, as the earliest branch of Pan-Cyclanorbinae instead, rather than nested within Plastomenidae. This placement of *A. superstes* and *A. foveatus* is supported by one unambiguous apomorphy; 1(4). The position of *A. infernalis* as sister-taxon to Cyclanorbinae + Plastomenidae is then supported by a single apomorphy; 24(1).

We present a new Bayesian topology in Figure 9B (the Bayesian log file is available in Appendix 5). As in Evers et al. (2023), the Bayesian topology is markedly different from the parsimony topology concerning the contents of the Trionychidae stem-group (Figure 9). This stem is formed successively by a clade containing *Perochelys lamadongensis* Li, Joyce, and Liu, 2015, *P. hengshanensis* Brinkman, Rabi, and Zhao, 2017, *Kuhnemys maortuensis* Yeh, 1965, and *Petrochelys kyrgyzensis* Nessov, 1995, and *Gobiapalone orlovi* as the sister-taxon to crown-Trionychidae (Figure 9B). Notably, and contrary to the Bayesian topology of Evers et al. (2023), we do not recover *Axestemys infernalis* as the sister-taxon to crown-Cyclanorbinae. Instead, we find reasonably strong support that the clade containing *Hutchemys* spp. Joyce et al., 2009, and *Helopanoplia distincta* is closer to Cyclanorbinae than *A. infernalis* (Figure 9B). *A. infernalis* is recovered as closer to Cyclanorbinae than to Plastomenidae, but support for this placement is weak. As in the parsimony tree, the position of *A. infernalis* is supported by a single apomorphy; 24(1).

DISCUSSION

Interspecific Variation in *Axestemys infernalis*

We note various differences between the four crania attributed to *Axestemys infernalis* (Table 1). MAB13742 differs from all other *A. infernalis* specimens by maxilla-jugal suture posterior to orbit, ventrally expanded postorbital and jugal not superficially contributing to the posterior margin of the orbit in lateral view. MAB13742 differs from DMNH 98814 and NSM PV24650 by unossified premaxillae, a condition that cannot be confirmed in DMNH 130951. MAB13742 differs from NSM PV24650 by the lack of cranial sculpturing. The lat-

TABLE 1. Selected character variation between known crania of *Axestemys infernalis*.

Character	DMNS 98814	DMNS 130951	NSM PV24650	MAB 13742
Premaxilla - quadrate condyle length	14.5 cm	15.0 cm	16.0 cm	9.8 cm
Skull roof surface	smooth	smooth	sculptured	smooth
Postorbital expanded ventrally	no	no	no	yes
contact maxilla - jugal, relative to orbit	ventral	ventral	ventral	posterior
Excavation dorsal surface ane	absent	extensive	modest	modest
Premaxilla ossified	yes	?	yes	no
Ventral surface of maxilla, lateral view	straight	rounded	straight	rounded
Prefrontal - frontal suture	straight	straight	triangular	fused
Basisphenoid - palatine contact present	yes	no	yes	?

eral excavation of the dorsal surface of the naris in MAB13742 most resembles that of NSM PV24650 - not as extensive as in DMNH 130951 but more apparent than in DMNH 98814. Other documented variation between *A. infernalis* crania includes the contact between palatines and basisphenoid, which is present in DMNH 98814 and NSM PV24650 but not in DMNH 130951 (Joyce et al., 2019). This condition in MAB13742 is unclear, as the sutures on the ventral side are not visible through our CT-scan.

Cranial sculpturing is present in all other species of *Axestemys* (Vitek, 2012; Vitek and Joyce, 2015; Georgalis and Joyce, 2017), and was even considered a synapomorphy of the genus (Vitek and Joyce, 2015; Georgalis and Joyce, 2017). However, within *A. infernalis*, this character state is only present in NSM PV24650. The degree of skull roof sculpturing is used as an indication for skeletal maturity in various sauropsid groups like squamates and archosaurs, whereby typically sculpturing increases through ontogeny (Griffin et al., 2020). This ontogenetic variation has not been tested in turtles yet. Nonetheless, NSM PV24650 is interpreted to be the most mature specimen of *A. infernalis* on the basis of cranial proportions (Joyce et al., 2019), so that the presence of sculpturing in NSM PV24650 as a consequence of its skeletal maturity is consistent with other sauropsids.

The lack of a premaxilla in MAB13742 (Figure 2) can be explained either by a lack of a premaxilla altogether, a cartilaginous premaxilla that did not preserve, or loss through breakage. The premaxillae in trionychids, when present, are fused into a small element that does not extend dorsally to the apertura narium externum (Meylan, 1987). This fusion occurs early in trionychid development (Sánchez-Villagra et al., 2009), but their ossification is delayed with respect to other turtle clades (Sheil, 2003; Sánchez-Villagra et al., 2009). Meylan (1987) observed the lack of a premaxilla in some trionychid specimens, but his survey included dried skulls only. It is plausible that these instances of a missing premaxilla reflect a cartilaginous premaxilla in life that did not preserve in the dried skull. If MAB13742 bore an ossified premaxilla in life, that was later lost through breakage, it seems unlikely that the narrow bridge ventral to the apertura narium externum, currently formed by the maxilla, would remain. For instance, this entire structure is broken off in DMNH 130591. We therefore interpret that the absence of a premaxilla in MAB13742 reflects a cartilaginous premaxilla in life.

Interspecific variation in the position of the maxilla-jugal suture is also documented in *Gilmoremys lancensis* Gilmore, 1916, a plastomenid turtle from the Hell Creek and Lance formations of which seven crania have been described (Joyce and Lyson, 2011; Joyce et al., 2016). While the suture is positioned ventral to the orbit in most specimens, BMRP 2013.4.214 from Montana displays this suture posterior to the orbit (Joyce et al., 2016; Figure 2C). In this specimen, the jugal reaches the orbit by a dorsoventrally narrow process wedged between the maxilla and a dorsoventrally narrow postorbital. In MAB13742, the superficial exclusion of the jugal to the orbit is seemingly caused by a ventral expansion of the postorbital. This ventral expansion of the postorbital is not seen in *G. lancensis*. It is possible that a jugal-orbit contact is reached in MAB13742 medially to the postorbital, but the CT-scan resolution was insufficient to observe the maximum anterior extent of the jugal. Complete absence of a jugal-orbit contact is highly unusual and found only in *Cycloderma aubryi* Duméril, 1856, among Trionychia (Meylan, 1987).

A contact between the basisphenoid and palatines is plesiomorphically present in crown-Trionychia, and subsequent loss occurred independently in few species (Meylan, 1987). This loss may be

limited to a subsection of the population in some species. Joyce et al. (2019) show that such a contact is prevented by the pterygoid in *Axestemys infernalis* DMNH 130951. Apart from *A. infernalis, Gilmoremys lancensis* represents the only other crown-trionychian taxon in which this character varies intraspecifically, as absence of the contact is observed in MRF 277 (Joyce et al., 2011).

Potential Causes of Intraspecific Cranial Variation

Intraspecific variation has been well-documented in various extant trionychids (Webb, 1962; Dalrymple, 1977; Meylan, 1987; Gardner and Russell, 1994). Joyce et al. (2019) discuss three potential causes of intraspecific variation observed in *Axestemys infernalis*, but take into account only the variation of the shell as they do not deem the cranial variation in their sample of three skulls significant. Generally, larger turtles possess better-developed shell callosities than smaller turtles. However, within the sample of *A. infernalis*, this trend is not as clear-cut, exemplified by the following two end-members (Joyce et al., 2019): the Turtle Bonebed locality preserves small individuals (carapace length below 45 cm) with well-developed callosities. On the other hand, turtles preserved at the Big Turtle Cove locality are much larger (carapace length up to 75 cm) yet display poorly developed callosities. To explain this discrepancy, Joyce et al. (2019) proposed three potential causes: sexual dimorphism, habitat partitioning, and time averaging. We build upon these hypotheses and further discuss them in the context of cranial variation and propose ontogenetic variation as a fourth hypothesis explaining variation in the cranium.

Sexual dimorphism. In fully aquatic turtles as Trionychidae, females are significantly larger than males (Berry and Shine, 1980; Meylan, 1987). This sexually dimorphic size discrepancy is also present in the Eocene carettochelyid trionychian *Allaeochelys crassesculpta* Harrassowitz, 1922 (Joyce et al., 2012), suggesting a widespread distribution of this feature among Trionychia. However, Joyce et al. (2019) refuted that interspecific variation in shell size of *Axestemys infernalis* can be explained due to sexual dimorphism alone, as that would indicate single-sex aggregates in the Turtle Bonebed and Big Turtle Cove localities. In the context of cranial variation, morphometric analyses of extant trionychid crania did not yield significant sexual dimorphism either (e.g., Dalrymple, 1977; Taşkavak, 1998), so that we reject the sexual dimorphism hypothesis.

Habitat partitioning. In a twist on Pritchard's (2001) hypothesis on interspecific size variation within Trionychidae due to habitat partitioning, Joyce et al. (2019) suggested it is plausible that size difference may occur intraspecifically through habitat partitioning as well. This is consistent with sedimentological evidence and implies that differently sized individuals would have inhabited different habitats (Joyce et al., 2019). Smaller individuals preferred backwater habitats as preserved in the Turtle Bonebed locality, whereas larger specimens inhabited larger channel environments that are preserved in the Big Turtle Cove locality (Joyce et al., 2019). However, this hypothesis does not explain the presence of more skeletally mature individuals at the Turtle Bonebed locality (Joyce et al., 2019).

Time averaging. This hypothesis holds that the observed variation is due to random walk over the course of the depositional window of the Hell Creek and Lance Formations. It suggests that the turtles evolved in response to short-term changes and reflect favourable versus unfavourable conditions. In practice, this would imply that the turtles of the Turtle Bonebed locality developed during harsh times and remained small, while the Big Turtle Cove individuals lived during times that are more advantageous and were able to reach larger sizes. This hypothesis also accounts for intermediate forms present.

In order to test whether certain characters evolved over the course of the Hell Creek-Lance depositional window, it is key to compare the stratigraphic levels of the *Axestemys infernalis* crania. Both DMNH 98814 and DMNH 130951 are recovered from sites near the base of the Hell Creek Formation at Slope County, North Dakota; the Turtle Ridge and Big Turtle Cove localities, respectively (Joyce et al., 2019). Big Turtle Cove is lower relative to the Hell Creek-Fort Union formational contact than the Turtle Ridge locality. NSM PV24650 was recovered at Sandy Site in Harding County, South Dakota (Joyce et al., 2019), of which the exact horizon has not been published. Similar to the North Dakota specimens, MAB13742 was found at the base of the Lance Formation. However, the precise horizon is unclear. Correlation between noncontinuous outcrops of the Hell Creek and Lance formations is very difficult, as these outcrops are lithologically indistinguishable, and the vertical position of a given channel differs per time (Fastovsky, 1987; Murphy et al., 2002). As such, direct age correlation between neither MAB13742 and the North Dakota specimens nor NSM

PV24650 is possible with the data at hand. Therefore, at present, there is insufficient data to explore the cranial evolution of *A. infernalis*.

Ontogeny. We propose ontogeny as a fourth option, to explain some of the observed cranial variation. Cranial anatomy is known to vary depending on individual size and feeding ecology; structures related to feeding, such as muscle attachment sites, increase allometrically with age in extant *Apalone ferox* Schneider, 1783 (Dalrymple, 1977, therein *Trionyx ferox*). Similar ontogenetic features are present in *G. lancensis* (Joyce et al., 2016), whereby juveniles possessed a narrow skull with a narrow processus trochlearis oticum while more mature individuals had widely expanded the skull and processus trochlearis oticum. Consistent with these cranial proportions, Joyce et al. (2019) inferred that DMNH 98814 represents the most juvenile individual of *A. infernalis* and NSM PV24650 the most mature. DMNH 130951 seemingly fits between these two extremes and appears most similar to each other in size and overall dimensions. MAB13742 is significantly smaller than the other reported crania of *A. infernalis*. However, in terms of overall dimensions, it is most comparable to DMNH 130591. Ferreira et al. (2022) recently demonstrated allometric growth of braincase endocasts in turtles; juvenile braincase endocasts are round and compact, whereas this structure becomes more elongate in adults. From the elongate shape of the braincase endocast in MAB13742 (Figure 7), we infer that MAB13742 has reached a stage at which the braincase endocast shape is fully developed. Nonetheless, NSM PV24650 appears more mature in terms of size and overall proportions, notably the wider processus trochlearis oticum. The presence of cranial sculpturing in NSM PV24650 alone, as an indicator of skeletal maturity, is consistent with the pattern in other sauropsids (Griffin et al., 2020).

Due to the limited sample size, conclusive evidence is lacking for any hypothesis. The ontogenetic hypothesis at least addresses the distribution of cranial sculpturing, being present only in the most mature NSM PV24650. However, it does not seem to explain any other character.

Intraspecific Cranial Variation in *Axestemys*

While the genus *Axestemys* currently contains seven species (Vitek, 2012; Vitek and Joyce, 2015; Georgalis and Joyce, 2017; Joyce et al., 2019), only four species are known with sufficient cranial material preserved; *A. infernalis* (Joyce et al., 2019), *A. splendida* (Gardner et al., 1995), *A. montinsana* (Vitek, 2012), and *A. vittata* (Moody and Walker, 1970; Walker and Moody, 1985, therein *Eurycephalochelys fowleri*). The anatomical variation discussed below is summarised in Table 2.

Axestemys splendida represents the only other Cretaceous species of *Axestemys* (Joyce et al., 2019). Gardner et al. (1995) reconstructed the cranium of *A. splendida* (therein *Aspideretoides*

TABLE 2. Selected character variation between known crania of *Axestemys* species.

Character	*A. infernalis*	*A. splendida*	*A. montinsana*	*A. vittata*
Skull outline	triangular to wide	triangular	triangular	wide
Triturating surface	smooth	?	rugose	smooth
Orbit size	large	large	large	small
Jugal bar origin	level of orbit	level of orbit	level of orbit	ventral to orbit
Skull roof sculpturing	absent or present	present	present	present
Ventral margin of maxilla	rounded or straight	rounded	horizontal	straight slope
Anterior flange of quadrate inclination	oblique	?	?	near-horizontal
Opening fpp	enclosed in palatine	between palatine and maxilla	?	lateral to ascending process palatine
Prefrontal - frontal suture	variable	straight	straight	triangular
Contribution of parietal to processus trochlearis oticum	>20%	reduced	>20%	?
Maxilla deep	yes	yes	yes	yes
Postorbital over complete length of postorbital bar	yes	yes	yes	yes
Maxillae form a secondary palate	no	no	no	no

splendidus) based on two specimens, TMP 90.59.01 and UALVP 5000, and provided a brief description. *A. splendida* resembles *A. infernalis* in the following characters: large size (basicranial length 11.0 - 12.0 cm). Deep maxilla. Moderately broad triturating surface. Maxillae do not form a secondary palate. A postorbital that extends over the entire postorbital bar anteroposteriorly. However, the two taxa are different in the following characters: The contribution of the prootic and quadrate to the processus trochlearis oticum is enhanced in *A. splendida*, while that of the parietal is reduced. In *A. infernalis* the parietal makes up more than 20% of the processus trochlearis oticum. The basisphenoid broadly contacts the palatines in both specimens of *A. splendida*, a character that is more variable in *A. infernalis*. Both cranial specimens of *A. splendida* display cranial sculpturing (Vitek, 2012).

Axestemys infernalis resembles *A. montinsana* UMMP 27029 in the following cranial characters: blunt and deep maxillae. A postorbital that extends over the entire postorbital bar anteroposteriorly. A parietal that makes up more than 20% of the processus trochlearis oticum. High crista supraoccipitalis. Wide triturating surfaces (Vitek, 2012). Maxillae do not form a secondary palate. Vitek (2012) also noted a weakly emarginated dorsolateral edge of the apertura narium externa and contact between the basisphenoid and palatines as similarities, but these characters appear to be more variable in *A. infernalis. A. montinsana* is currently differentiated from other *Axestemys* by the unique combination of the following characters: a blunt and triangular skull and a rugose triturating surface (Vitek and Joyce, 2015). We note that the ventral margin of the maxilla is horizontal, in contrast to the rounded to gently sloping condition in *A. infernalis* and the gently sloping condition in *A. vittata*. Additionally, the prefrontal-frontal suture is straight, rather than the triangular suture in *A. vittata*.

Axestemys vittata has had a complex taxonomic history. Pomel (1847) described *Trionyx vittatus* on a now lost holotype carapace (Broin, 1977). Moody and Walker (1970) described an incomplete cranium BMNH R8445, which they assigned to the new genus *Eurycephalochelys fowleri*. Broin (1977) reassigned *Trionyx vittatus* to *Palaeotrionyx vittatus*, based on similarity to the American genus *Paleotrionyx* Schmidt, 1945, but misspelled the generic name. *Palaeotrionyx vittatus* was later synonymized with *Eurycephalochelys* to form *Eurycephalochelys vittatus* (Augé et al., 1997). Following Vitek (2012), Georgalis and Joyce (2017) referred these taxa to *Axestemys* but deemed that the variation observed was insufficient to maintain two species, and hence named *Axestemys vittata* - emending the species epithet to *vittata* to conform the feminine gender of -emys. Independently, Walker and Moody (1985) had extended the generic diagnosis of *"Eurycephalochelys"* based data on more complete crania, most notably BMNH R8694.

Regarding this diagnosis, *Axestemys vittata* resembles *A. infernalis* in the following cranial characters: Large size (premaxilla – occipital condyle length 15.7 – 23.4 mm). Maxilla very deep, being two-thirds as deep as vertical diameter of orbit. Maxillae do not form a secondary palate. Maximum width of skull across jugal bars equal to width across articular region of quadrates. Area of quadrate exposed on dorsal surface not larger than area of prootic but of approximately equal size. Quadrate condyles situated posterior to foramen stapedio-temporale. Tympanic cavity shallow and triangular in outline. Foramen magnum, and brain cavity immediately anterior to it, rounded. Postorbital extends over entire postorbital bar anteroposteriorly.

However, there are a number of notable differences between *Axestemys vittata* and *A. infernalis* based on the diagnosis of *"Eurycephalochelys fowleri"* (Walker and Moody, 1985). The orbits of *A. vittata* are significantly smaller than in *A. infernalis*. As a result, the jugal bar originates below the orbit in *A. vittata*. In *A. vittata*, the anterior opening of the foramen palatinum posterius is situated to the side of the ascending process of palatine rather than enclosed in bone as in *A. infernalis*. *A. vittata* is characterised by a forwardly-directed flange of the quadrate that is inclined more horizontal than other trionychids.

All cranial specimens described above share the following characters: (1) Deep maxillae. (2) Postorbital that extends over the entire postorbital bar antero-posteriorly. (3) Maxillae do not form secondary palate. However, the descriptions highlight that *Axestemys* displays notable interspecific cranial variation. More detailed taxonomic studies on *Axestemys* cranial anatomy are advised.

Phylogeny of Trionychia and Placement of *Axestemys*

Vitek (2012) initially placed members of *Axestemys* as crown-trionychines, in a clade with *Aspideretoides* spp. and *Oliveremys uintaensis* Leidy, 1873, that forms the sister-group to *Apalone* +

Rafetus. Subsequent analyses of trionychian phylogeny did not include any *Axestemys* species. Evers et al. (2023) were the first to include *Axestemys infernalis* in a phylogenetic analysis of Pan-Trionychia but did not include other *Axestemys* species. In both the parsimony and Bayesian analysis, *A. infernalis* was placed within Pan-Cyclanorbinae and their Bayesian analysis recovered *A. infernalis* as the sister-taxon to crown-Cyclanorbinae. Although no unambiguous character states were found in support of this *Axestemys*-Cyclanorbinae sister-relation, DELTRAN optimizations in support included the absence of a dorsolateral emargination of the external naris. This coding does not reflect the entire spectrum of *A. infernalis*, as Joyce et al. (2019) noted a 'minor' dorsolateral emargination in DMNH 130951. With this character state updated, *A. infernalis* is no longer recovered as the sister-taxon to crown-Cyclanorbinae (Figure 8). Swapping the branches of *A. infernalis* with that of *Helopanoplia distincta* + *Hutchemys* spp. ultimately does not affect stratigraphic congruence. Both *A. infernalis* and *H. distincta* are limited to the Maastrichtian Hell Creek and Lance formations (Joyce and Lyson, 2017; Joyce et al., 2019), whereas the included *Hutchemys* species range from the Maastrichtian to the Palaeocene-Eocene boundary (Joyce et al., 2009; Jasinski et al., 2022).

Notably, the contents of the clade Plastomenidae vary between the parsimony and Bayesian analyses. In the PhyloCode, Joyce et al. (2021) maintain a definition for Plastomenidae as "the largest extinct clade including *Plastomenus* (orig. *Trionyx*) *thomasii* (Cope, 1872)". As the clade consisting of *Atoposemys* and *Aspideretoides* is recovered as the earliest branching Pan-Cyclanorbinae in the parsimony analysis (Figure 8A), these taxa are excluded from Plastomenidae according to this analysis.

CONCLUSIONS

We report the first trionychid cranium from the Maastrichtian Lance Formation of Wyoming, MAB13742, which we assign to *Axestemys infernalis* based on its large size, blunt and deep maxillae, triturating surfaces that do not form a secondary palate, and a postorbital that extends over the entire anteroposterior length of the postorbital bar. This specimen differs from the previously published skulls of *A. infernalis* by the lack of an ossified premaxilla, a ventrally expanding postorbital, and the maxilla contacting the jugal posterior to the orbit. Our updated phylogenetic analysis place *A. infernalis* either outside the Plastomenidae+Cyclanorbinae clade, or as early branching stem-Cyclanorbinae, but never as the direct sister-taxon to crown-Cyclanorbinae. Moreover, there is considerable inter- and intraspecific variation in cranial material assigned to *Axestemys*, and further taxonomic studies of this genus are advised.

ACKNOWLEDGEMENTS

We like to thank G. Georgalis and one anonymous reviewer for their helpful and constructive comments on an earlier draft of the manuscript. We are grateful to the ranchers who allowed us to conduct fieldwork on their land, which made it possible to discover and collect this specimen. The CT-scanning team from the Jeroen Bosch Ziekenhuis, in particular B. Ketelaars, kindly helped us with the scanning of the specimen. We also thank W.G. Joyce (Université de Fribourg) for providing photographs of additional cranial specimens of *Axestemys*. In addition, W.G. Joyce, R.B. Sookias and the Jörg Fröbisch Lab at the Museum für Naturkunde Berlin are thanked for helpful discussions. We thank J. P. Cavigelli from the Tate Museum Casper for aiding the fieldwork. JP was funded by an Elsa-Neumann Stipendium.

REFERENCES

Agassiz, L. 1857. Contributions to the natural history of the United States of America. First Monograph. Vol 1, Part 1. Essay on Classification. Part II. North American Testudinata. Boston: Little Brown and Co., 1:1–452. https://doi.org/10.5962/bhl.title.12644

Augé, M., Duffaud, S., de Lapparent de Broin, F., Rage, J.-C., and Vasse, D. 1997. Les amphibiens et les reptiles de Prémontré (Cuisien, Bassin parisien): une herpétofaune de reference pour l'Eocène inférieur. Géologie de la France, 1:23–33.

Baur, G. 1891. On the relations of *Carettochelys*, Ramsay. American Naturalist, 25:631–639. https://doi.org/10.1086/275363

Bell, T. 1828. Characters of the order, families, and genera of the Testudinata. Zoological Journal, 3:513–516.
Berry, J.F. and Shine, R. 1980. Sexual size dimorphism and sexual selection in turtles (order Testudines). Oecologica, 44(2):185–191. https://doi.org/10.1007/bf00572678
Boddaert, P. 1770. Brief van de kraakbenige schildpad. Epistola de testudine cartilaginea. Amsterdam: Kornelis van Tongerlo, 39 pp.
Brinkman, D., Rabi, M., and Zhao, L. 2017. Lower Cretaceous fossils from China shed light on the ancestral body plan of crown soft shell turtles (Trionychidae, Cryptodira). Scientific Reports, 7:6719. https://doi.org/10.1038/s41598-017-04101-0
Broin, F. 1977. Contribution à de l'étude des Chéloniens. Chéloniens continentaux du Crétacé Supérieur et de Tertiaire de France. Mémoires du Muséum National D'Histoire Naturelle, 38:1–366.
Cope, E.D. 1868. On the origin of genera. Proceedings of the National Academy of Sciences, 20:242–300. https://doi.org/10.1086/270388
Cope, E.D. 1872. Descriptions of some vertebrate from the Bridger Group of the Eocene. Proceedings of the American Philosophical Society, 12:460–465.
Cope, E.D. 1874. Review of the Vertebrata of the Cretaceous Period found west of the Mississippi River. Bulletin of the United States Geological and Geographical Survey of the Territories, First Series, 2:3–48.
Dalrymple, G.H. 1977. Intraspecific variation in the cranial feeding mechanism of turtles of the genus *Trionyx* (Reptilia, Testudines, Trionychidae). Journal of Herpetology, 11(3):255–285. https://doi.org/10.2307/1563241
Danilov, I.G., Hirayama, R., Sukhanov, V.B., Suzuki, S., Watabe, M., and Vitek, N.S. 2014. Cretaceous soft-shelled turtles (Trionychidae) of Mongolia: new diversity, records and a revision. Journal of Systematic Palaeontology, 12(7):799–832. https://doi.org/10.1080/14772019.2013.847870
Daudin, F.M. 1802. Histoire naturelle, generale et particuliere, des Reptiles, Paris, 2:1–432
Duméril, A.H.A. 1856. Note sur les reptiles du Gabon. Revue et Magasin de Zoologie Pure et Appliquée, Paris, 2(8):369–377.
Edgar, S.C., Brinkman, D.B., Ryan, M.J., and Evans, D.C. 2021. A new plastomenid trionychid (Testudines: Pan-Trionychidae) from Milk River Formation of Southern Alberta (Cretaceous: Santonian). Canadian Journal of Earth Sciences, 59(4):205–215. https://doi.org/10.1139/cjes-2021-0040
Engstrom, T.N., Shaffer, H.B., and McCord, W.P. 2004. Multiple data sets, high homoplasy, and the phylogeny of softshell turtles (Testudines: Trionychidae). Systematic Biology, 53(5):693–710. https://doi.org/10.1080/10635150490503053
Evers, S.W. 2021. 3D Models related to the publication: Evers, S.W., Joyce, W.G., Choiniere, J.N., Ferreira, G.S., Foth, C., Hermanson, G., Hongyu, Y., Johnson, C.M., Werneburg, I., and Benson, R.B.J. 2022. Independent origin of large labyrinth size in turtles. Nature communications, 13:5807. https://doi.org/10.1038/s41467-022-33091-5
Evers, S.W., Neenan, J.M., Ferreira, G.S., Werneburg I., Barrett, P.M., and Benson, R.B.J. 2019. Neurovascular anatomy of the protostegid turtle *Rhinochelys pulchriceps* and comparisons of membranous and endosseous labyrinth shape in an extant turtle. Zoological Journal of the Linnean Society, 187(3):800–828. https://doi.org/10.1093/zoolinnean/zlz063
Evers, S.W., Ponstein, J., Jansen, M.A., Gray, J.A., and Fröbisch, J. 2022. A systematic compendium of turtle mandibular anatomy using digital dissections of soft tissue and osteology. The Anatomical Record, 306(6):1228–1303. https://doi.org/10.1002/ar.25037
Evers, S.W., Chapelle, K.E.J., and Joyce, W.G. 2023. Cranial and mandibular anatomy of *Plastomenus thomasii* and a new time-tree of trionychid evolution. Swiss Journal of Palaeontology, 142:1–40. https://doi.org/10.1186/s13358-023-00267-5

Fastovsky, D.E. 1987. Paleoenvironments of vertebrate-bearing strata During the Cretaceous-Paleogene Transition, Eastern Montana and Western North Dakota. Palaios, 2:282–295. https://doi.org/10.2307/3514678

Ferreira, G.S., Werneburg, I., Lautenschlager, S., and Evers, S.W. 2021. 3D Models related to the publication: Contrasting brains and bones: neuroanatomical evolution of turtles (Testudinata), p. 79–121. In Dozo, M.T., Paulina-Carabajal, A., Macrini, T.E., and Walsh, S. (eds.), Paleoneurology of Amniotes: new directions in the study of fossil endocasts. Springer Cham, Switzerland.

Ferreira, G.S., Werneburg, I., Lautenschlager, S., and Evers, S.W. 2022. Contrasting brains and bones: neuroanatomical evolution of turtles (Testudinata), p. 79–121. In Dozo, M.T., Paulina-Carabajal, A., Macrini, T.E., and Walsh, S. (eds.), Paleoneurology of Amniotes: New Directions in the Study of Fossil Endocasts. Springer Cham, Switzerland. https://doi.org/10.1007/978-3-031-13983-3_4

Gaffney, E.S. 1979a. Comparative cranial morphology of recent and fossil turtles. Bulletin of the American Museum of Natural History, 164(2):65–376.

Gaffney, E.S. 1979b. Description of a large trionychid turtle shell from the Eocene Bridger Formation of Wyoming. Contributions to Geology, University of Wyoming, 17:53–57.

Gardner, J.D. and Russell, A.P. 1994. Carapacial variation among soft-shelled turtles (Testudines: Trionychidae), and its relevance to taxonomic and systematic studies of fossil taxa. Neues Jahrbuch für Geologie und Palaontologie-Abhandlungen, 193(2):209–244. https://doi.org/10.1127/njgpa/193/1994/209

Gardner, J.D., Russell, A.P., and Brinkman, D.B. 1995. Systematics and taxonomy of soft-shelled turtles (Family Trionychidae) from the Judith River Group (mid-Campanian) of North America. Canadian Journal of Earth Science, 32:631–643. https://doi.org/10.1139/e95-053

Georgalis, G.L. 2021. First pan-trionychid turtle (Testudines, Pan-Trionychidae) from the Palaeogene of Africa. Papers in Palaeontology, 7(4):1919–1926. https://doi.org/10.1002/spp2.1372

Georgalis, G.L. and Joyce, W.G. 2017. A review of the fossil record of Old World turtles of the clade Pan-Trionychidae. Bulletin of the Peabody Museum of Natural History, 58:115–208. https://doi.org/10.3374/014.058.0106

Gill, T. 1889. A remarkable tortoise. In Annual Report of the Board of Regents of the Smithsonian Institution, for the Year Ending June 30th, 1887, 1:509–511.

Gilmore, C.W. 1916. Description of two new species of turtles, from the Lance Formation of Wyoming. Proceedings of the United States National Museum, 50(2137):614–646. https://doi.org/10.5479/si.00963801.50-2137.641

Goloboff, P.A. and Catalano, S. 2016. TNT, version 1.5, including a full implementation of phylogenetic morphometrics. Cladistics, 32(3):221–238. https://doi.org/10.1111/cla.12160

Harrassowitz, H. 1922. Die Schildkrötengattung *Anosteira* von Messel bei Darmstadt und ihre stammesgeschichtliche Bedeutung. Abhandlungen der Hessischen Geologischen Landesanstalt zu Darmstadt, 6(3):133–238.

Hay, O.P. 1899. On the names of certain American fossil vertebrates. American Geologist, 24:345–349. https://doi.org/10.1126/science.9.225.593

Hay, O.P. 1902. Bibliography and catalogue of the fossil vertebrata of North America. Bulletin of the United States Geological Survey, 179:1–868. https://doi.org/10.5962/bhl.title.20094

Hay, O.P. 1908. The fossil turtles of North America. Carnegie Institution of Washington, Publication, 75:1–568. https://doi.org/10.5962/bhl.title.12500

Head, J.J., Aguilera, O.A., and Sánchez-Villagra, M.R. 2006. Past colonization of South America by trionychid turtles: fossil evidence from the Neogene of Margarita Island, Venezuela. Journal of Herpetology, 40(3):378–381. https://doi.org/10.1670/0022-1511(2006)40[378:PCOSAB]2.0.CO;2

Hummel, K. 1929. Die fossilen Weichschildkröten (Trionychia). Eine morphologisch-systematische und stammesgeschichtliche Studie. Geologische und Paläontologische Abhandlungen, 16:359–487

Jasinski, S.E., Heckert, A.B., Sailar, C., Lichtig, A.J., Lucas, S.G., and Dodson, P. 2022. A softshell turtle (Testudines: Trionychidae: Plastomeninae) from the uppermost Cretaceous (Maastrichtian) Hell Creek Formation, North Dakota, USA, with implications for the evolutionary relationships of plastomenines and other trionychids. Cretaceous Research, 135:105172. https://doi.org/10.1016/j.cretres.2022.105172

Joyce, W.G. and Lyson, T.R. 2010. A neglected lineage of North American turtles fills a major gap in the fossil record. Palaeontology, 53(2):241–248. https://doi.org/10.1111/j.1475-4983.2009.00929.x

Joyce, W.G. and Lyson, T.R. 2011. New material of *Gilmoremys lancensis* nov. comb. (Testudines: Trionychidae) from the Hell Creek Formation and the diagnosis of plastomenid turtles. Journal of Paleontology, 85(3):442–459. https://doi.org/10.1666/10-127.1

Joyce, W.G., Micklich, N., Schaal, S.F.K., and Scheyer, T.M. 2012. Caught in the act: the first record of copulating fossil vertebrates. Biology Letters, 8:846–848. https://doi.org/10.1098/rsbl.2012.0361

Joyce, W.G., Lyson, T.R., and Williams, S. 2016. New cranial material of *Gilmoremys lancensis* (Testudines, Trionychidae) from the Hell Creek Formation of southeastern Montana, U.S.A. Journal of Vertebrate Paleontology, e1225748. https://doi.org/10.1080/02724634.2016.1225748

Joyce, W.G. and Lyson, T.R. 2017. The shell morphology of the latest Cretaceous (Maastrichtian) trionychid turtle *Helopanoplia distincta*. PeerJ, 5:e4169. https://doi.org/10.7717/peerj.4169

Joyce, W.G., Lyson, T.R., and Sertich, J.J.W. 2018. A new species of trionychid turtle from the Upper Cretaceous (Campanian) Fruitland Formation of New Mexico, USA. Journal of Paleontology, 92(6):1107–1114. https://doi.org/10.1017/jpa.2018.30

Joyce, W.G., Brinkman, D.B., and Lyson, T.R. 2019. A new species of trionychid turtle, *Axestemys infernalis* sp. nov., from the Late Cretaceous (Maastrichtian) Hell Creek and Lance formations of the Northern Great Plains, USA. Palaeontologia Electronica, 22.3.72:1–28. https://doi.org/10.26879/949

Joyce, W.G., Anquetin, J., Cadena, E.-A., Claude, J., Danilov, I.G., Evers, S.W., Ferreira, G.S., Gentry, A.D., Georgalis, G.L., Lyson, T.R., Pérez-García, A., Rabi, M., Sterli, J., Vitek, N.S., and Parham, J.F. 2021. A nomenclature for fossil and living turtles using phylogenetically defined clade names. Swiss Journal of Palaeontology, 140(5):1–45. https://doi.org/10.1186/s13358-020-00211-x

Khosatzky, L.I. 1976. [A new representative of trionychids from the Late Cretaceous of Mongolia]. Gerpetologiya. Kubanskiy Gosudarstvennyy Universitetskye Nauchnye Trudy, 218:3–19. [In Russian]

Klein, I.T. 1760. Klassification und kurze Geschichte der vierfüßigen Thiere (translation by F. D. Behn). Lübeck: Jonas Schmidt.

Lautenschlager, L., Ferreira, G.S., and Werneburg, I. 2018. Sensory evolution and ecology of early turtles revealed by digital endocranial reconstructions. Frontiers in Ecology and Evolution, 6(7):1–16. https://doi.org/10.3389/fevo.2018.00007

Le, M., Duong, H.T., Dinh, L.D., Nguyen, T.Q., Pritchard, P.C.H., and McCormack, T. 2014. A phylogeny of softshell turtles (Testudines: Trionychidae) with reference to the taxonomic status of the critically endangered, giant softshell turtle, *Rafetus swinhoei*. Organisms Diversity & Evolution, 14(3):279–293. https://doi.org/10.1007/s13127-014-0169-3

Leidy, J. 1873. Notice of donation of fossils, etc., from Wyoming. Proceedings of the Academy of Natural Sciences of Philadelphia, 24:267–268.

Li, L., Joyce, W.G., and Liu, J. 2015. The first soft-shelled turtle from the Jehol Biota of China. Journal of Vertebrate Paleontology, e909450-2. https://doi.org/10.1080/02724634.2014.909450

Lydekker, R. 1889. Catalogue of fossil Reptilia and Amphibia in the British Museum. Part III. Chelonia. London: British Museum of Natural History. https://doi.org/10.1086/275366

Lyson, T.R., Petermann, H., and Miller, I.M. 2021. A new plastomenid trionychid turtle, *Plastomenus joycei*, sp. nov., from the earliest Paleocene (Danian) Denver Formation of south-central Colorado, U.S.A. Journal of Vertebrate Paleontology, 41:e1913600. https://doi.org/10.1080/02724634.2021.1913600

Meylan, P.A. 1987. The phylogenetic relationships of soft-shelled turtles (family Trionychidae). Bulletin of the American Museum of Natural History, 186:1–101.

Meylan, P.A. and Gaffney, E.S. 1989. The skeletal morphology of the Cretaceous cryptodiran turtle, *Adocus*, and the relationships of the Trionychoidea. American Museum Novitates, 2941:1–60.

Moody, R.T.J. and Walker, C.A. 1970. A new trionychid turtle from the British Lower Eocene. Palaeontology, 13(3):503–510.

Murphy, E.C., Hoganson, J.W., and Johnson, K.R. 2002. Lithostratigraphy of the Hell Creek Formation in North Dakota. In Hartman, J.H., Johnson, K.R., and Nichols, D.J. (eds.), The Hell Creek Formation and the Cretaceous-Tertiary boundary in the northern Great Plains: An integrated continental record of the end of the Cretaceous: Boulder, Colorado, Geological Society of America, Special Paper, 361:9–34. https://doi.org/10.1130/0-8137-2361-2.9

Nessov, L.A. 1995. Dinozavri severnoi Yevrazii: Novye dannye o sostave kompleksov, ekologii i paleobiogeografii. Institute for Scientific Research on the Earth's Crust, St. Petersburg State University, St. Petersburg.

Pomel, A. 1847. Note sur les mammifères et reptiles fossiles des terrains éocènes de Paris, inférieurs au dépôt gypseux. Archives des Sciences Physiques et Naturelles de Genève, 4:326–330.

Pritchard, P.C.H. 2001. Observations on body size, sympatry, and niche divergence in softshell turtles (Trionychidae). Chelonian Conservation and Biology, 4:5–27.

Ramsay, E.P. 1887. On a new genus and species of fresh water tortoise from the Fly River, New Guinea. Proceedings of the Linnean Society of New South Wales, 2:158–162.

Rhodin, A.G.J., Iberson, J.B., Bour, R., Fritz, U., Georges, A., Shaffer, H.B., and van Dijk, P.P. 2021. Turtles of the world: Annotated checklist and atlas of taxonomy, synonymy, distribution, and conservation status. In Rhodin, A.G.J., Iverson, J.B., van Dijk, P.P., Stanford, C.B., Goode, E.V., Buhlmann, K.A., and Mittermeier, R.A. (eds.), Conservation biology of freshwater turtles and tortoises: A compilation project of the UUCN/SSC tortoise and freshwater turtle specialist group (Vol. 8, 9th ed., pp. 1–472). Chelonian Research Monographs. https://doi.org/10.3854/crm.8.checklist.atlas.v9.2021

Ronquist, F., Van der Mark, P., and Huelsenbeck, J.P. 2009. Bayesian phylogenetic analysis using Mr Bayes, p. 210–266. In Lemey, P., Salemi, M., and Van Damme, A.M. (eds.), The phylogenetic handbook 2. Cambridge: Cambridge University Press.

Russell, L.S. 1930. A new species of Aspideretes from the Paskapoo Formation of Alberta. American Journal of Science, 115:27–32.

Sánchez-Villagra, M.R., Asher, R.J., Rincón, A.D., Carlini, A.A., Meylan, P.A., and Purdy, R.W. 2004. Fossils of the Miocene Castillo Formation, Venezuela: contributions on neotropical palaeontology. Special Papers in Palaeontology, 71:105–112. https://doi.org/10.1017/s0016756805300781

Sánchez-Villagra, M.R., Müller, H., Sheil, C.A., Scheyer, T.M., Nagashima, H., and Kuratani, S. 2009. Skeletal development in the Chinese soft-shelled turtle *Pelodiscus sinensis* (Testudines: Trionychidae). Journal of Morphology, 270:1381–1389. https://doi.org/10.1002/jmor.10766

Scheyer, T.M., Mörs, T., and Einarsson, E. 2012. First record of soft-shelled turtles (Cryptodira, Trionychidae) from the Late Cretaceous of Europe. Journal of Vertebrate Paleontology, 32:1027–1032. https://doi.org/10.1080/02724634.2012.685036

Schmidt, K.P. 1945. A new turtle from the Paleocene of Colorado. Fieldiana Geology, 10:1–4. https://doi.org/10.5962/bhl.title.3383

Schneider, J.G. 1783. Allgemeine Naturgeschichte des Schildkröten, nebst einem systematischen Verzeichnisse der einzelnen Arten und zwey Kupfern. J.G. Müller, Leipzig. https://doi.org/10.5962/bhl.title.5788

Sheil, C.A. 2003. Osteology and skeletal development of Apalone spinifera (Reptilia: Testudines: Trionychidae). Journal of Morphology, 256:42–78. https://doi.org/10.1002/jmor.10074

Smith, E.N. and Gutberlet, R.L. 2001. Generalized Frequency Coding: a method of preparing polymorphic multistate characters for phylogenetic analysis. Systematic Biology, 50(2):156–169.

Taşkavak, E. 1998. Comparative morphology of the Euphrates soft-shelled turtle, *Rafetus euphraticus* (Daudin, 1802) (Reptilia, Testudines) in Southeastern Anatolia. Amphibia-Reptilia, 19:281–291. https://doi.org/10.1163/156853898x00188

Thomson, R.C., Spinks, P.Q., and Shaffer, H.B. 2021. A global phylogeny of turtles reveals a burst of climate-associated diversification on continental margins. PNAS, 118(7):e2012215118. https://doi.org/10.1073/pnas.2012215118

Vitek, N.S. 2012. Giant fossil soft-shelled turtles of North America. Palaeontologia Electronica, 15.1.13A:1–43. https://doi.org/10.26879/299

Vitek, N.S. and Joyce, W.G. 2015. A review of the fossil record of New World turtles of the clade Pan-Trionychidae. Bulletin of the Peabody Museum of Natural History, 56(2):185–244. https://doi.org/10.3374/014.056.0204

Walker, C.A. and Moody, R.T.J. 1985. Redescription of *Eurycephalochelys*: a trionychid turtle from the Lower Eocene of England. Bulletin of the British Museum of Natural History, 38(5):373–380

Walther, W.G. 1922. Die Neu-Guinea-Schildkröte *Carettochelys insculpta* Ramsay: Dissertation zur Erlangung der Doktorwürde bei der Philosophischen Fakultät der Hessischen Ludwigs-Universität zu Giessen. Brill, Leiden.

Webb, R.G. 1962. North American Recent soft-shelled turtles. University of Kansas Publications, Museum of Natural History, 13(10):429–611.

Werneburg I., Evers, S.W., and Ferreira, G.S. 2021a. 3D models related to the publication: On the “cartilaginous rider” in the endocasts of turtle brain cavities. MorphoMuseuM, 7(148). https://doi.org/10.18563/journal.m3.146

Werneburg I., Evers, S.W., and Ferreira, G.S. 2021b. On the “cartilaginous rider” in the endocasts of turtle brain cavities. Vertebrate Zoology, 71:403–418. https://doi.org/10.3897/vz.71.e66756

Wiegmann, A.F.A. 1835. Beiträge zur Zoologie, gesammelt auf einer Reise um die Erde, von Dr. F.J.F.Meyen. Siebente Abhandlung. Amphibien. Nova Acta Academiae Caesarae Leopoldina Carolinae Germanicae Naturae Curisorum, 17:183–268.

Yeh, H.K. 1965. New materials of fossil turtles of Inner Mongolia. Vertebrata Palasiatica, 9:47–69.

APPENDIX 1.

Changes to character scores

Changes to OTUs

Axestemys infernalis, supplement scoring with specimen MAB13742

Changes to scores

Axestemys infernalis
Character 31 (1 -> 1&2)
Apertura narium externum is dorsolaterally excavated in some specimens, especially in DMNH 130951
Character 44 (1 -> 2)
Premaxilla unossified in specimen MAB13742
Character 99 (? -> 2)
Observed in specimen MAB13742

Character 33
Likely character states are swapped in character 33. Absence (state 1) in outgroup *Adocus* (e.g., Meylan and Gaffney 1989), that is correct. Presence (state 2) correctly coded in *Carretochelys insculpta* (e.g., Walther 1922; Joyce 2014). But in remaining extant taxa, the coding is swapped. Absence of basisphenoid-palatine contact is diagnostic among extant trionychids for *Rafetus euphraticus* (Meylan 1987), but in the matrix of Evers et al. (2023) is only extant taxon coded with presence (state 2).

Cyclanorbis elegans
Character 33 (1 -> 2)

Cyclanorbis senegalensis
Character 33 (1 -> 2)

Cycloderma aubryi
Character 33 (1 -> 2)

Cycloderma frenatum
Character 33 (1 -> 2)

Lissemys punctata
Character 33 (1 -> 2)

Trionyx triunguis
Character 33 (1 -> 2)

Chitra indica
Character 33 (1 -> 2)

Pelochelys bibroni
Character 33 (1 -> 2)

Rafetus euphraticus
Character 33 (2 -> 1)

Apalone ferox
Character 33 (1 -> 2)

Apalone spinifera
Character 33 (1 -> 2)

Apalone mutica
Character 33 (1 -> 2)

Dogania subplanus
Character 33 (1 -> 2)

Nilssonia formosus
Character 33 (1 -> 2)

Nilssonia hurum
Character 33 (1 -> 2)

Nilssonia gangetica
Character 33 (1 -> 2)

Amyda cartilaginea
Character 33 (1 -> 2)

Palea steindachneri
Character 33 (1 -> 2)

Pelodiscus sinensis
Character 33 (1 -> 2)

Gobiapalone orlovi
Character 33 (1 -> 2)
Presence observed in MPC 25/160 (Danilov et al. 2014)

REFERENCES

Danilov, I.G., Hirayama, R., Sukhanov, V.B., Suzuki, S., Watabe, M., and Vitek, N.S. 2014. Cretaceous soft-shelled turtles (Trionychidae) of Mongolia: new diversity, records and a revision. Journal of Systematic Palaeontology, 12(7):799–832. https://doi.org/10.1080/14772019.2013.847870

Evers, S.W., Chapelle, K.E.J., and Joyce, W.G. 2023. Cranial and mandibular anatomy of *Plastomenus thomasii* and a new time-tree of trionychid evolution. Swiss Journal of Palaeontology, 142:1–40. https://doi.org/10.1186/s13358-023-00267-5

Joyce WG. 2014. A review of the fossil record of turtles of the clade Pan-*Carettochelys*. Bulletin of the Peabody Museum of Natural History 55: 3-33

Meylan, P.A. 1987. The phylogenetic relationships of soft-shelled turtles (family Trionychidae). Bulletin of the American Museum of Natural History, 186: 1–101.

Meylan, P.A. and Gaffney, E.S. 1989. The skeletal morphology of the Cretaceous cryptodiran turtle, Adocus, and the relationships of the Trionychoidea. American Museum Novitates, 2941:1–60

Walther, W.G. 1922. Die Neu-Guinea-Schildkröte *Carettochelys insculpta* Ramsay: Dissertation zur Erlangung der Doktorwürde bei der Philosophischen Fakultät der Hessischen Ludwigs-Universität zu Giessen

APPENDIX 2.

List of characters

Updates to character matrix (Evers et al. 2023)

Reworded characters

Character 44. Premaxilla absent. 1: no, 2: occasionally, 3: usually

to:

Character 44. Premaxilla ossified. 1: yes, 2: usually, 3: occasionally

Character 100 of Evers et al. (2023) was not transferred to actual character matrix.

Two characters were labelled as Character 111

Modified character list

Character 1: Width-length of nuchal bone. 1 = less than 2; 2 = greater than 2; 3 = greater than 3; 4 = greater than 4.

Character 2: Anterior and posterior costiform processes of nuchal bone united. 1 = no; 2 = yes.

Character 3: Position of anterior edge of first body vertebra relative to nuchal bone. 1 = posterior edge of nuchal; 2 = middle of nuchal; 3 = anterior edge of nuchal.

Character 4: First and second neurals fused. 1 = no; 2 = yes.

Character 5: Total number of peripherals. 1 = 22; 2 = 20; 3 = 14-18; 4 = 0.

Character 6: Prenuchal bone. 1 = absent; 2 = present.

Character 7: Size of eighth pleurals. 1 = large; 2 = reduced or absent.

Character 8: Epiplastral callosity. 0 = absent; 1 = present.

Character 9: Entoplastral callosity. 0 = absent; 1 = present.

Character 10: Hyo/Hypoplastral callosity. 0 = absent; 1 = present.

Character 11: Xiphiplastral callosity. 0 = absent; 1 = present.

Character 12: Supernumerary callosities. 0 = absent; 1 = present.

Character 13: Hyoplastra and hypoplastra fuse just after hatching. 1 = no; 2 = yes.

Character 14: Extended midline contact of xiphiplastral callosities. 1 = absent; 2 = present along much of the midline.

Character 15: Hypo-xiphiplastral union. 1 = xiphiplastra lateral to hypoplastra; 2 = hypoplastra lateral to xiphiplastra.

Character 16: Number of neurals. 1 = eight ; 2 = seven ; 3 = six or less.

Character 17: Variability in position of neural reversal. 1 = always at same neural; 2 = always at adjacent neurals; 3 = highly variable.

Character 18: Pleurals which meet at midline. 0 = none; 1 = eighth only; 2 = seventh and eighth or eighth only; 3 = sixth, seventh, and eighth or seventh and eighth; 4 = sixth, seventh, and eighth or seventh and eighth.

Character 19: Point of reversal of orientation of neurals. 1 = seven ; 2 = six; 3 = five; 4 = four.

Character 20: Suprascapular fontanelles. 1 = closed at hatching; 2 = closed in large adults only; 3 = open throughout life.

Character 21: Epiplastron shape. 1 = J-shaped; 2 = I-shaped.

Character 22: Length epiplastra anterior to entoplastron contact. 1 = short; 2 = intermediate; 3 = long.

Character 23: Depressions on eighth pleurals for contact of ilia. 1 = present; 2 = absent.

Character 24: Bridge length. 1 = long; 2 = short.

Character 25: Largest adult size 200 mm or less (disc length). 1 = no; 2 = yes.

Character 26: Carapace margin straight to concave posteriolaterally. 1 = no; 2 = yes.

***Character 27**: Sexual dimorphism in disc length. 1 = no; 2 = yes.

Character 28: Jugal contacts squamosal. 1 = no; 2 = in one half of sample.

Character 29: Jugal contacts parietal on skull surface. 1 = no; 2 = yes.

Character 30: Vomer contacts prefrontal. 1 = yes; 2 = no.

Character 31: Dorsal edge of aperture narium externum laterally emarginated. 1 = no; 2 = weakly; 3 = strongly.

Character 32: Dorsal edge of aperture narium externum medially emarginated. 1 = no; 2 = yes.

Character 33: Basisphenoid contacts palatines. 1 = no; 2 = yes.

Character 34: Vomer divides maxillae. 1 = yes; 2 = no.

Character 35: Vomer reaches intermaxillary foramen. 1 = yes; 2 = no.

Character 36: Vomer contacts basisphenoid. 1 = no; 2 = occasionally.

Character 37: Size of foramen palatinum posterius. 1 = large; 2 = small; 3 = small and divided; 4 = many small openings.

Character 38: Foramen jugulare posterius. 1 = open; 2 = enclosed.

Character 39: Contribution of pterygoid to bar separating foramen julare posterius. 0 = absent; 1 = present.

Character 40: Foramen posterius canalis carotici interni relative to lateral crest of basioccipital tubercle. 1 = above; 2 = in it; 3 = below.

Character 41: Maxilla contacts frontal in front of orbit. 1 = no; 2 = yes.

Character 42: Exoccipital contacts pterygoid. 1 = no; 2 = yes.

Character 43: Basisphenoid shape. 1 = not medially constricted; 2 = medially constricted.

Character 44: Premaxilla absent. 1 = no; 2 = occasionally; 3 = usually.

Character 45: Vomer lost. 1 = no; 2 = yes.

Character 46: Jugal contacts orbit. 1 = yes; 2 = no.

Character 47: Epipterygoid, if present, contacts the palatine. 1 = yes; 2 = no.

Character 48: Contact between pterygoid and foramen nervi trigemini occurs when epipterygoid is present. 1 = yes; 2 = no.

Character 49: When epipterygoid is present pterygoid contacts foramen nervi trigemini. 0 = between epipterygoid and quadrate or not at all; 1 = between prootic and epipterygoid or not at all; 2 = between epipterygoid and parietalor not at all.

Character 50: Epipterygoid contacts prootic anterior to foramen nervi trigemini. 1 = no; 2 = yes.

Character 51: Epipterygoid contacts prootic posterior to foramen nervi trigemini. 1 = no; 2 = yes.

Character 52: Epipterygoid fuses to pterygoid. 1 = in subadults; 2 = in adults only; 3 = never.

Character 53: Average ratio of intermaxillary foramen length to length primary palate. 0 = 0.07; 1 = 0.20 to 0.402 = about 0.60.

Character 54: Postorbital bar relative to orbit. 0 = about 2 times orbit diameter; 1 = about equal to orbit to 1/3 of orbit2 = less than 1/5 of orbit.

Character 55: Proportion of processus trochlearis oticum made up by parietal. 1 = 15.6% or less; 2 = 22.1% or more.

Character 56: Ventral keel on 8th cervical present and limited to posterior end. 1 = no; 2 = yes.

Character 57: Strong dorsal processes on cervicals. 1 = no; 2 = yes.

Character 58: Number of ossifications in corpus hyoidis. 1 = 6; 2 = 8.

Character 59: Number of ossifications in comu branchiale II. 1 = 1 only; 2 = 44714; 3 = 7 or more.

Character 60: Ossifications of comu branchiale II broad and strongly sutured. 1 = no; 2 = yes.

Character 61: Basihyals in close contact and projecting anteriorly. 1 = no; 2 = yes.

Character 62: Symphyseal ridge strong and present in a depression. 1 = no; 2 = yes.

Character 63: Foramen intermandibularis caudalis. 0 = absent; 1 = present at least in parts of the population.

Character 64: Ilia curve medially. 1 = no; 2 = yes.

Character 65: Ischia extend into thyroid fenestra. 1 = yes; 2 = no.

Character 66: Metischial processes present and distinct. 1 = yes; 2 = no.

Character 67: Angle of acromion process to scapula approaches that of coracoid to acromion. 1 = no; 2 = yes.

Character 68: Coracoid longest of three pectoral processes. 1 = no; 2 = yes.

Character 69: Development of surface sculpturing of carapace and plastron. 0 = all metaplastic portions of carapace and plastron have trionychid sculpturing; 1 = trionychid pattern grades towards the center of carapacial and plastral disk to a smooth pattern, as developed in Hutchemys rememdium and Hutchemys arctochelys.

Character 70: Nuchal notch. 0 = anterior rim of nuchal convex or slightly notched; 1 = anterior rim of carapace with deep nuchal notch, as developed in H. rememdium.

Character 71: Shape of neural 1 and 2 (neural 2 and 3 of Meylan 1987). 0 = neurals 1 and 2 hexagonal with short posterior sides; 1 = neural 1 circular to rectangular and neural 2 octagonal, as developed in H. rememdium and H. arctochelys.

Character 72: Splitting of costals along distal margin. 0 = costal rim rounded or graded; 1 = dorsal rims split into separately protruding dorsal and visceral portions, as developed in H. rememdium and H. arctochelys.

Character 73: Lateral notch in carapace at the level of costal 5. 0 = absent, lateral carapacial margin rounded; 1 = present, lateral carapacial margin shows a waist, as developed in H. arctochelys.

Character 74: Skin callosity developed on the visceral side of costals 6 and 7. 0 = absent, visceral side smooth; 1 = present, visceral side sometimes develops a callosity, as seen in H. arctochelys.

Character 75: Mid-line contact of hyoplastra, hypoplastra and xiphiplastra. 0 = hyo-, hypo- and xiphiplastra do not contact another fully, even in adults; 1 = hyo-, hypo and xiphiplastra contact another fully along the entire mid-line in adults, as developed in H. rememdium and H. arctochelys.

Character 76: Shape of deep portion of entoplastron. 0 = lateral branches of entoplastron more or less straight and merge anterior at a clear angle; 1 = entoplastron wide and rounded, as seen in P. aff. thomasii.

Character 77: Mobility of entoplastron and anterior development of hyoplastron. 0 = lateral branches of entoplastron abut loosely against hyoplastron, anterior rim of hyoplastron develops no anterior flap/shoulder; 1 = lateral branches of entoplastron abut loosely against hyoplastron, but hyoplastron develops an anterior flap/shoulder, as seen in Plastomenus aff. thomasii; 2 = entoplastron tightly integrated into anterior plastral lobe due to strong development of anterior flap/shoulder, as developed in H. rememdium and H. arctochelys.

Character 78: Peripheral ossification. 0 = lateral bridge ossification of plastron does not significantly extend beyond the lateral processes of hyo- and hypoplastron; 1 = lateral bridge ossification of plastron extends laterally beyond bridge processes of the hyo- and hypoplastron and ossifies the peripheral aspects of the shell, as seen in H. arctochelys.

Character 79: Number of lateral hyoplastral processes. 1 = one; 2 = two; 3 = three or more.

Character 80: Extensive secondary palate consisting of infolded maxillae. 0 = absent; 1 = present, as developed in Plastomenus thomasii.

Character 81: Accessory ridges of upper triturating surfaces. 0 = absent; 1 = present.

Character 82: Dentary symphysis. 0 = short; 1 = extremely long, mandible extremely elongate, as developed in Plastomenus thomasii.

Character 83: Parietal contribution to orbits. 0 = parietals neither contribute to orbit margins or orbit walls; 1 = parietals either contribute to orbit walls, as developed in Gilmoremys lancensis, or orbit margin, as developed in Plastomenus thomasii.

Character 84: Proportions of costals VIII. 0 = wider than long to nearly square; 1 = significantly taller than wide.

Character 85: Hyoplastron with strongly serrated medial edge. 0 = present; 1 = absent.

Character 86: Serrated medial edge of hyoplastron extends nearly to the posterior edge of bone. 0 = present; 1 = absent.

Character 87: Process on medial edge of hypoplastron. 0 = of subequal size and radiating outward from the medial edge of the bone; 1 = with enlarged anterior process separated by a gap from smaller posterior processes.

Character 88: Ossification of basibranchials. 0 = poorly ossified, especially posterior pair ; 1 = well ossified.

Character 89: Metaplastic ossification of hypoplastron "rolls" onto posterior aspects of lateral processes. 0 = absent; 1 = present.

Character 90: Free rib ends. 0 = all ribs end free, not covered by metaplastic ossification; 1 = only costal ribs VII and VIII free; 2 = all ribs covered by metaplastic bone.

***Character 91**: Carapacial striations in adults. 0 = absent; 1 = present.

Character 92: Contribution of opisthotic to bar separating foramen jugulare posterius: 0 = absent; 1 = present.

Character 93: Contribution of excoccipital to bar separating foramen jugulare posterius: 0 = absent; 1 = present.

Character 94: Fusion of frontals: 0 = absent; 1 = present.

Character 95: Jugal, jugal participation in the margin of the upper temporal emargination: 0 = absent; 1 = present, upper temporal emargination extensive.

Character 96: Jugal, contact with the pterygoid: 0 = absent; 1 = present.

Character 97: Postorbital: 0 = completely reduced; 1 = present.

Character 98: Maxilla, well-developed suborbital crest: 0 = absent; 1 = present.

Character 99: Maxilla, Supraalveolar foramen (on the medial surface of the maxilla within the nasal capsule): 0 = absent; 1 = present, with posteriorly developed groove; 2 = present as fenestra-like opening into the supraalveolar canal.

Character 100: Premaxilla/vomer, foramen praepalatinum: 0 = absent; 1 = present.

Character 101: Foramina in vomer (possibly praepalatine foramina): 0 = absent; 1 = present.

Character 102: Anterior palate region, vomer and or premaxillae/maxillae, transversely concave ventral surface (‘tongue groove’) on anterior parts between maxillae: 0 = absent; 1 = present.

Character 103: Quadrate, infolding ridge on the posterior surface of the quadrate ventral to the incisura columella auris: 0 = absent or extremely minor; 1 = ridge present but low; 2 = ridge present and forms massive overhanging flange. Ordered.

Character 104: Pterygoid, pterygoid contribution to foramen palatinum posterius: 0 = absent; 1 = present.

Character 105: Maxilla, maxilla contribution to foramen palatinum posterius: 0 = absent; 1 = present.

Character 106: Pterygoid, lateral flange at lateral margin: 0 = absent; 1 = present.

Character 107: Parabasisphenoid, abducens nerve course: 0 = in fully ossified canal; 1 = in dorsally open groove.

Character 108: Prootic, lateral semicircular canal enclosure by bone: 0 = canal only formed by bone of the opisthotic, the prootic portion of the canal is not ossified and is instead medially confluent with the recessus labyrinthicus prooticus; 1 = prootic and opisthotic both contribute to the formation of the lateral semicircular canal.

Character 109: Position of the foramen posterius canalis carotici interni (fpcci): 0 = the fpcci is located at the ventral surface of the skull in a position far anterior to the margin of the fenestra postotica; 1 = the fpcci is located at the posterior end of the skull, either on the ventral surface of the skull close to the margin of the fenestra postotica, or on the posterior surface of the skull at the ventral margin of the fenestra postotica.

Character 110: Dentary, expansion of lingual margin: 0 = absent; 1 = lingual margin is medially expanded to a shelf, which often is broader along the central part of the mandibular ramus than near the coronoid and symphyseal ends; 2 = lingual margin is so far expanded that it forms a huge, spatulate continuous surface with the symphysis.

Character 111: Dentary, size of foramen dentofaciale majus: 0 = absent, foramen completely reduced; 1 = small, size of a small vessel; 2 = enlarged, foramen is several mm in diameter.

Character 112: Dorsal surangular foramen: 0 = absent; 1 = present.

Character 113: Coronoid, foramen at anterior end, leading from fossa Meckelii into space between mandibular rami: 0 = absent; 1 = present.

Character 114: Prearticular, exposure of foramen alveolare inferius in medial view: 0 = absent, the foramen is covered by expansions of the prearticular and/or coronoid; 1 = present, the foramen can be seen in medial view.

Character 115: Anterior intermandibular foramen: 0 = absent; 1 = present, fully or partially formed between the angular and prearticular along their anterior processes. Note that this character is scored as inapplicable when the anteroventral process of the prearticular is absent.

Character 116: Posterior chorda tympani foramen: 0 = located within the articular notch on the posterior surface of the articular; 1 = located on the posteromedial jaw surface, usually on the prearticular or prearticular-articular contact.

Character 117: Articulation facet, contribution of prearticular: 0 = absent, prearticular completely retracted from articulation facet; 1 = prearticular forms small medial portion of articulation facet.

APPENDIX 3.

Character matrix. Appendix 3-5 are available for download at https://palaeo-electronica.org/content/2024/5234-new-skull-of-axestemys

APPENDIX 4.

MrBayes script. Appendix 3-5 are available for download at https://palaeo-electronica.org/content/2024/5234-new-skull-of-axestemys

APPENDIX 5.

Bayesian log file. Appendix 3-5 are available for download at https://palaeo-electronica.org/content/2024/5234-new-skull-of-axestemys